

Causation between Smoking and DNA methylation

1 **Twin-based Mendelian Randomization Analyses Highlight Smoking's Effects** 2 **on Blood DNA Methylation, with Putative Reverse Causation**

3
4 Madhurbain Singh^{1,2,3*}, Conor V. Dolan^{3,4}, Dana M. Lapato^{1,2}, Jouke-Jan Hottenga^{3,4}, René
5 Pool^{3,4}, Brad Verhulst⁵, Dorret I. Boomsma^{3,4,12}, Charles E. Breeze^{6,7}, Eco J. C. de Geus^{3,4},
6 Gibran Hemani⁸, Josine L. Min⁸, Roseann E. Peterson^{9,10,1}, Hermine H. M. Maes^{1,2}, Jenny van
7 Dongen^{3,4,11*}, and Michael C. Neale^{1,2,3,11*}

- 8
9 1. Virginia Institute for Psychiatric and Behavioral Genetics, Department of Psychiatry,
10 Virginia Commonwealth University, Richmond, VA, USA
11 2. Department of Human and Molecular Genetics, Virginia Commonwealth University,
12 Richmond, VA, USA
13 3. Department of Biological Psychology, Vrije Universiteit (VU) Amsterdam, Amsterdam,
14 The Netherlands
15 4. Amsterdam Public Health Research Institute, Amsterdam, The Netherlands
16 5. Department of Psychiatry and Behavioral Sciences, Texas A&M University, College
17 Station, TX, USA
18 6. Division of Cancer Epidemiology and Genetics, National Cancer Institute, National
19 Institutes of Health, Department Health and Human Services, Bethesda, MD, USA
20 7. UCL Cancer Institute, University College London, London, UK.
21 8. MRC Integrative Epidemiology Unit, University of Bristol, Bristol, UK
22 9. Department of Psychiatry and Behavioral Sciences, SUNY Downstate Health Sciences
23 University, Brooklyn, NY, USA
24 10. Institute for Genomics in Health, SUNY Downstate Health Sciences University,
25 Brooklyn, NY, USA
26
27 11. These authors jointly supervised this work.
28 12. Current address: Department of Complex Trait Genetics, Center for Neurogenomics and
29 Cognitive Research, Vrije Universiteit (VU) Amsterdam, Amsterdam, The Netherlands

30
31 *Corresponding authors:

32 Madhurbain Singh. Email: singhm18@vcu.edu. Address: Virginia Institute for Psychiatric and
33 Behavioral Genetics, 800 E. Leigh St., Suite 100, Richmond, VA 23298, USA

34 Jenny van Dongen. Email: j.van.dongen@vu.nl. Address: Department of Biological Psychology,
35 Vrije Universiteit Amsterdam, van der Boechorststraat 7, 1081 BT Amsterdam, The Netherlands

36 Michael C. Neale. Email: michael.neale@vcuhealth.org. Address: Virginia Institute for
37 Psychiatric and Behavioral Genetics, 800 E. Leigh St., Suite 100, Richmond, VA 23298, USA

38

39 Running head: **Causation between smoking and DNA methylation**

Causation between Smoking and DNA methylation

40 **Table of Contents**

41	Funding.....	2
42	Acknowledgments.....	3
43	Conflicts of Interest.....	3
44	ORCID.....	3
45	Data Availability.....	3
46	Code Availability.....	4
47	<i>Abstract</i>	5
48	<i>Introduction</i>	6
49	<i>Results</i>	10
50	<i>cis</i> -mQTLs identified for two-thirds of smoking-associated CpG sites.....	10
51	Exemplar: Putative causality between current smoking and <i>AHRR</i> DNAm.....	13
52	Evidence of more widespread effects of current smoking on DNAm than <i>vice versa</i>	17
53	Suggestive Evidence of Bidirectional Effects at Four CpG Sites.....	23
54	DNAm loci potentially influenced by smoking are enriched for biological processes relevant to	
55	smoking's adverse health outcomes.....	25
56	CpG sites with consistent effects on current smoking show enrichment for brain-related gene regulatory	
57	elements.....	25
58	Attenuated effects of former smoking on DNAm.....	29
59	<i>Discussion</i>	31
60	<i>Methods</i>	34
61	Study Sample.....	34
62	Peripheral Blood DNA Methylation and Cell Counts.....	34
63	Cigarette Smoking.....	35
64	Instrumental Variables.....	35
65	MR-DoC Models.....	37
66	Functional Enrichment Analyses.....	39
67	eFORGE (experimentally derived Functional element Overlap analysis of ReGions from EWAS).....	39
68	<i>References</i>	41
69		

70 **Funding**

71 We acknowledge funding from the U.S. National Institute on Drug Abuse grant R01DA049867,
72 the Netherlands Organization for Scientific Research (NWO): Biobanking and Biomolecular
73 Research Infrastructure (BBMRI-NL, NWO 184.033.111) and the BBRMI-NL-financed BIOS
74 Consortium (NWO 184.021.007), NWO Large Scale infrastructures X-Omics (184.034.019),
75 Genotype/phenotype database for behavior genetic and genetic epidemiological studies (ZonMw
76 Middelgroot 911-09-032); Netherlands Twin Registry Repository: researching the interplay
77 between genome and environment (NWO-Groot 480-15-001/674); the Avera Institute, Sioux
78 Falls (USA), and the U.S. National Institutes of Health (NIH R01HD042157-01A1,
79 R01MH081802, R01MH125938, and Grand Opportunity grants 1RC2 MH089951 and 1RC2
80 MH089995). DML is supported by the NIH K01MH131847. DIB acknowledges the Royal

Causation between Smoking and DNA methylation

81 Netherlands Academy of Science Professor Award (PAH/6635). JLM and GH are supported by
82 the UK Medical Research Council (MRC) Integrative Epidemiology Unit at the University of
83 Bristol (MC_UU_00011/1, MC_UU_00011/5).

84 **Acknowledgments**

85 NTR warmly thanks all participants. Epigenetic data were generated at the Human Genomics
86 Facility (HuGe-F) at ErasmusMC Rotterdam (<http://www.glimdna.org/>) as part of the Biobank-
87 based Integrative Omics Study Consortium. We thank Dr. Scott Vrieze (University of
88 Minnesota) for providing the leave-one-out GWAS summary statistics from the GWAS &
89 Sequencing Consortium of Alcohol and Nicotine Use (GSCAN).

90 **Conflicts of Interest**

91 Nothing to declare.

92 **ORCID**

93 Madhurbain Singh: 0000-0002-9396-2860
94 Conor V. Dolan: 0000-0002-2496-8492
95 Dana M. Lapato: 0000-0001-8169-9754
96 Jouke-Jan Hottenga: 0000-0002-5668-2368
97 René Pool: 0000-0001-5579-0933
98 Brad Verhulst: 0000-0001-5369-9757
99 Dorret I. Boomsma: 0000-0002-7099-7972
100 Charles E. Breeze: 0000-0002-5294-915X
101 Eco J. C. de Geus: 0000-0001-6022-2666
102 Gibran Hemani: 0000-0003-0920-1055
103 Josine L. Min: 0000-0003-4456-9824
104 Roseann E. Peterson: 0000-0001-6402-849X
105 Hermine H. M. Maes: 0000-0001-7489-2214
106 Jenny van Dongen: 0000-0003-2063-8741
107 Michael C. Neale: 0000-0003-4887-659X

108 **Data Availability**

109 Data from the Netherlands Twin Register (NTR) may be accessed for research purposes by
110 submitting a data-sharing request. Further information about NTR data access is available at
111 <https://ntr-data-request.psy.vu.nl/>.

112

113 Results of all MR-DoC models fitted in this study are available as Supplementary Data.

Causation between Smoking and DNA methylation

114 **Code Availability**

115 The code used in the analyses for this study is available at: [https://github.com/singh-](https://github.com/singh-madhur/MRDOC_Smoking_DNA_m_NTR)
116 [madhur/MRDOC_Smoking_DNA_m_NTR](https://github.com/singh-madhur/MRDOC_Smoking_DNA_m_NTR).

117

118
119
120
121
122
123
124
125
126
127
128
129
130
131
132
133
134
135
136

Abstract

Epigenome-wide association studies (EWAS) aim to identify differentially methylated loci associated with complex traits and disorders. EWAS of cigarette smoking shows some of the most widespread DNA methylation (DNAm) associations in blood. However, traditional EWAS cannot differentiate between causation and confounding, leading to ambiguity in etiological interpretations. Here, we apply an integrated approach combining Mendelian Randomization and twin-based Direction-of-Causation analyses (MR-DoC) to examine causality underlying smoking-associated blood DNAm changes in the Netherlands Twin Register (N=2577). Evidence across models suggests that current smoking's causal effects on DNAm likely drive many of the previous EWAS findings, implicating functional pathways relevant to several adverse health outcomes of smoking, including hemopoiesis, cell- and neuro-development, and immune regulation. Additionally, we find evidence of potential reverse causal influences at some DNAm sites, with 17 of these sites enriched for gene regulatory functional elements in the brain. The top three sites with evidence of DNAm's effects on smoking annotate to genes involved in G protein-coupled receptor signaling (*GNG7*, *RGS3*) and innate immune response (*SLC15A4*), elucidating potential biological risk factors for smoking. This study highlights the utility of integrating genotypic and DNAm measures in twin cohorts to clarify the causal relationships between health behaviors and blood DNAm.

137

Introduction

138 Epigenome-wide association studies (EWASs) are valuable for identifying variation in DNA
139 methylation (DNAm) associated with complex human traits and diseases¹. By far, the most
140 successful EWASs have been the studies of cigarette smoking. A large-scale EWAS meta-
141 analysis of smoking (N = 15,907 individuals) compared current versus never smoking to reveal
142 significant DNAm differences at 18,760 CpG (*Cytosine-phosphate-Guanine*) sites in peripheral
143 blood cells². DNAm differences between former- and never-smoking individuals were
144 diminished but remained statistically significant at 2,568 sites². Genes annotated to the
145 differentially methylated CpG sites have been implicated in genome-wide association studies
146 (GWAS) of several smoking-associated traits, including cancers, lung functions, cardiovascular
147 disorders, inflammatory disorders, and schizophrenia, indicating DNAm's potential role in the
148 adverse health effects of smoking².

149

150 As cross-sectional EWAS in unrelated individuals cannot differentiate between causation and
151 confounding³, the widespread associations between cigarette smoking and DNAm² may originate
152 from a combination of different etiological mechanisms. These associations are typically
153 interpreted as the causal *effects* of smoking exposure on DNAm. However, some smoking-
154 associated CpG sites may have reverse or bidirectional causal links with smoking, such that
155 DNAm may reciprocally affect the development and maintenance of smoking behaviors⁴.
156 Moreover, associations between smoking and DNAm could be attributable to potential
157 confounders, such as schizophrenia⁵, alcohol consumption⁶, cannabis use⁷, and body mass
158 index⁸.

159

160 An alternative approach to causal inference in observational studies is Mendelian Randomization
161 (MR) analysis, using genetic variants as instrumental variables (IVs) to estimate causal effects
162 under specific assumptions^{3,9} (see **Methods**). Previous MR analyses have identified potential
163 effects of lifetime (current or former) smoking liability on blood DNAm at only 11 CpG sites¹⁰,
164 along with potential reverse effects of blood DNAm at 9 sites¹¹. The causal inference in MR is
165 based on the assumption that the genetic variants associated with the exposure influence the
166 outcome exclusively through the exposure. In other words, the genetic variants used as IVs for
167 smoking may show vertical pleiotropy, but not horizontal pleiotropy, with DNAm. To minimize
168 potential violations of these assumptions, MR analyses require carefully selected single-
169 nucleotide polymorphisms (SNPs), including using genetic colocalization to filter out SNPs
170 showing horizontal pleiotropy due to linkage disequilibrium (LD). Since individual SNPs usually
171 have minuscule effect sizes on complex traits, traditional MR approaches using a few selected
172 SNPs may have limited power to detect causality and may be subject to weak-instrument bias¹².

173

174 Recent methodological developments^{13,14} integrate the principles of MR with the twin-based
175 *Direction of Causation* model (hence called *MR-DoC*) from biometrical studies of mono- and
176 dizygotic twins¹⁵. Causal inference in twin data leverages the cross-twin cross-trait correlations

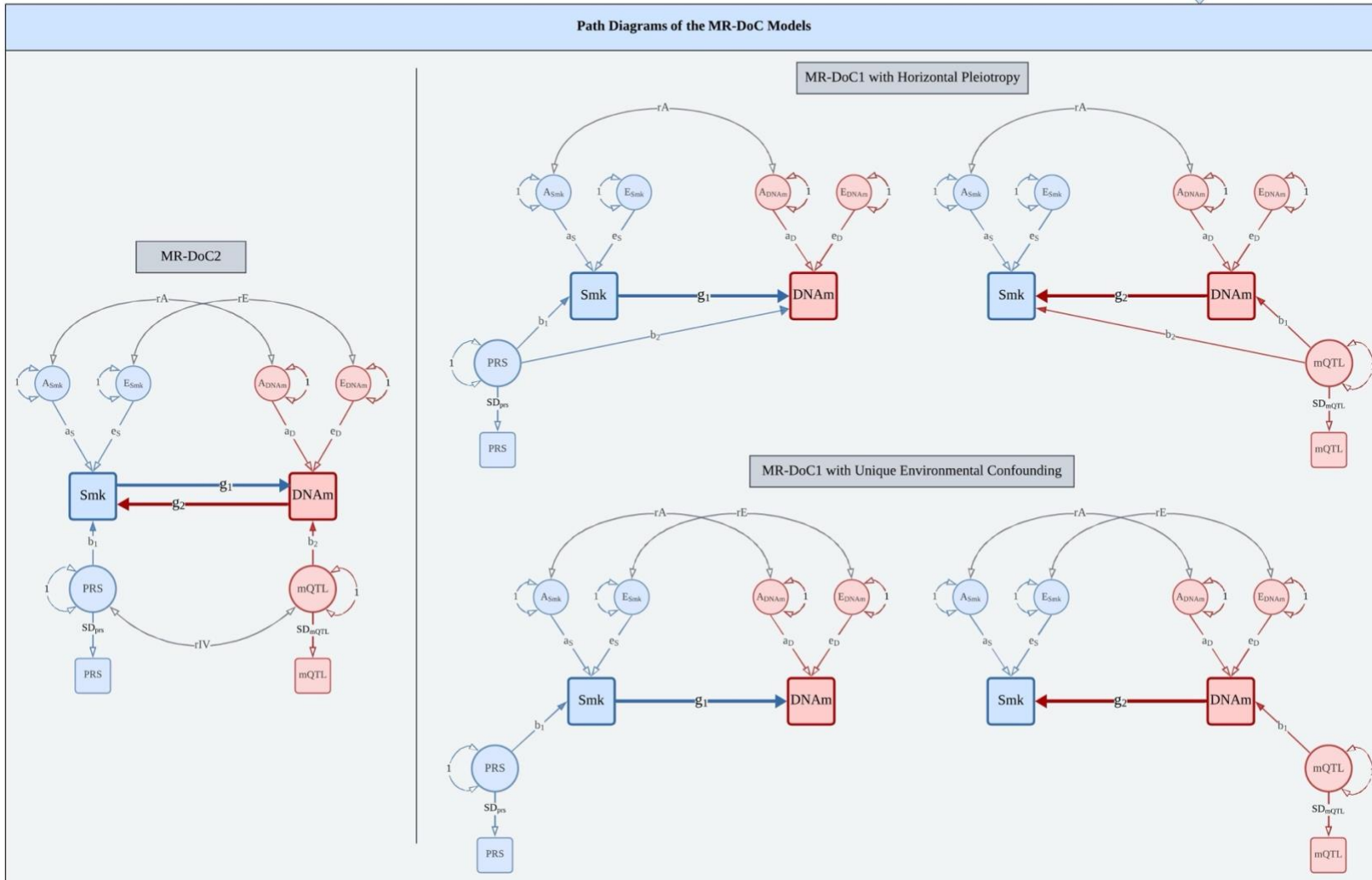
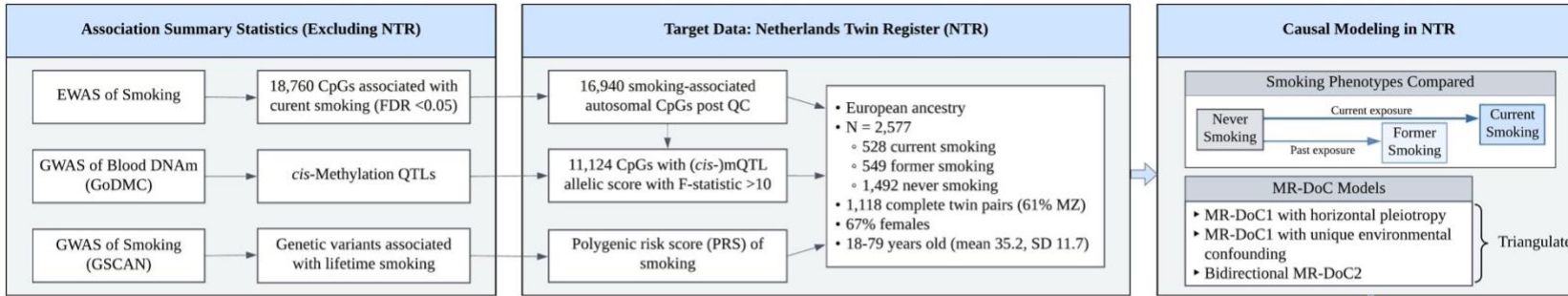
Causation between Smoking and DNA methylation

177 to estimate the direction and magnitude of potential causal effects between traits¹⁸. Further, the
178 MR-DOC approaches, i.e., the unidirectional *MR-DoC1*¹³ and the bidirectional *MR-DoC2*¹⁴, help
179 account for some of the horizontal pleiotropic associations of the genetic IV with the outcome,
180 unmediated by the exposure trait. Consequently, MR-DoC models allow using polygenic risk
181 scores (PRS) as potential IVs, increasing the statistical power to estimate causal effects while
182 curtailing weak-instrument bias relative to traditional MR methods that use SNPs as IVs.
183 Incorporating MR with family data also helps to resolve additional assumptions of standard MR,
184 such as random mating and no dyadic effects^{13,16}.

185
186 The present study used MR-DoC models to examine bidirectional causal effects between
187 cigarette smoking and peripheral blood DNAm in European ancestry adult twins from the
188 Netherlands Twin Register (NTR)¹⁷ (**Figure 1**). The target sample included 2,577 individuals
189 from 1,459 twin pairs with both genotypic and DNAm data, as well as their self-reported
190 smoking status at the time of blood draw (comprising 528 currently, 549 formerly, and 1,492
191 never-smoking individuals). Across 16,940 smoking-related CpGs previously identified², we
192 fitted separate models for current (versus never) and former (versus never) smoking. We
193 obtained a set of three causal estimates in each direction (*Smoking* → *DNAm*, and *DNAm* →
194 *Smoking*): the estimates from bidirectional MR-DoC2 and two different model specifications of
195 unidirectional MR-DoC1 (**Figure 1**). We triangulated evidence across the three models based on
196 the statistical significance and consistency of the causal estimates. The results indicated more
197 widespread putative causal influences of smoking on DNAm than *vice versa*. Follow-up
198 enrichment analyses highlighted biological processes and tissues relevant to the CpG sites with
199 potential effects in either direction of causation.

200

Causation between Smoking and DNA methylation



202 **Figure 1. Study Design.**

203 *Overview of the data and MR-DoC models used to examine the causality between cigarette smoking and blood DNA methylation (DNAm) in the*
204 *Netherlands Twin Register. The models were fitted separately for current (versus never) and former (versus never) smoking. Applying the five MR-*
205 *DoC models shown in the path diagrams, we obtained a set of three causal estimates in each direction of causation: Smoking (Smk) \rightarrow DNAm (the*
206 *blue paths labeled g_1) and DNAm \rightarrow Smoking (the red paths labeled g_2).*

207 *Note. For better readability, the path diagrams show only the within-individual part of the models fitted to data from twin pairs. The*
208 *squares/rectangles indicate observed variables, the circles indicate latent (unobserved) variables, the single-headed arrows indicate regression*
209 *paths, and the double-headed curved arrows indicate (co-)variances.*

210

Results

211 *cis*-mQTLs identified for two-thirds of smoking-associated CpG sites

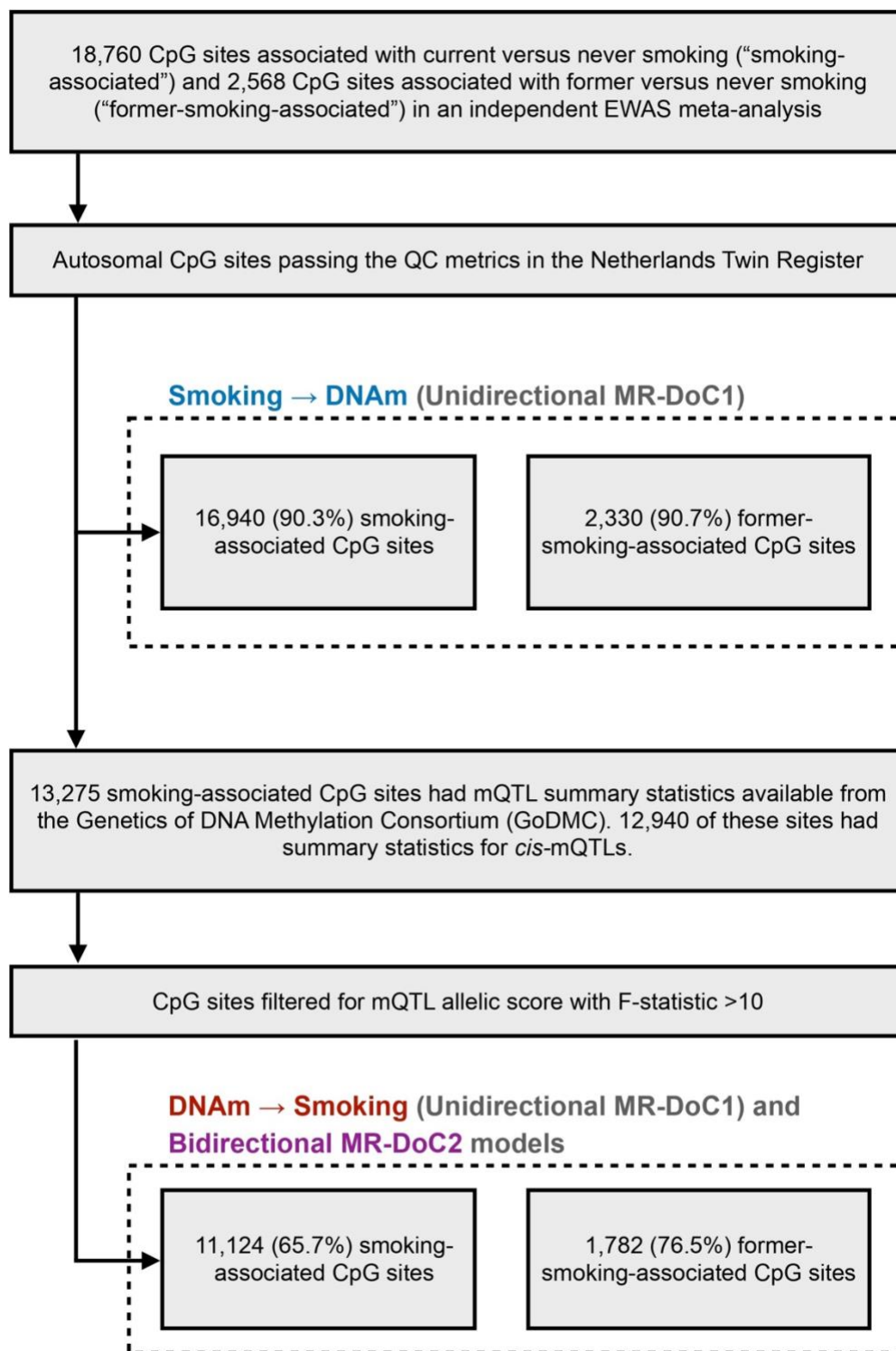
212 We used a weighted sum of relevant DNAm-increasing alleles at *cis*-methylation quantitative
213 trait loci (henceforth called *mQTL allelic score*) as the IV for DNAm. Of the 18,760 CpG sites
214 associated with current smoking in a previous independent EWAS meta-analysis², 16,940
215 autosomal sites passed the QC metrics in NTR (hereafter called the “smoking-associated CpGs”)
216 and were analyzed in the unidirectional MR-DoC1 models for *Current Smoking* → *DNAm*
217 (**Figure 2**). Of these sites, 13,275 had mQTL summary statistics from the Genetics of DNA
218 Methylation Consortium (GoDMC; excluding NTR)¹⁸. A subset of 12,940 sites had summary
219 statistics for *cis*-mQTLs, i.e., SNPs within 1Mb of the CpG. We used only *cis*-mQTLs to derive
220 the IVs for DNAm, given that SNPs located close to the CpG are more likely to be associated
221 with smoking *via* DNAm. To further guard against potential horizontal pleiotropy with smoking,
222 we relied on the consistency of the causal estimates in MR-DoC models accommodating
223 horizontal pleiotropy. To reduce the risk of weak-instrument bias in the estimated effects of
224 DNAm on smoking, we restricted the MR-DoC1 models for *DNAm* → *Current Smoking* and the
225 bidirectional MR-DoC2 models to 11,124 (65.7%) smoking-associated CpGs having an mQTL
226 allelic score with F-statistic >10, the criterion for the “relevance” assumption of a valid IV¹⁹ (see
227 **Methods**). The included mQTL allelic scores had an incremental R² for the respective CpG site
228 ranging from 0.43% to 76.95% (mean 9.04%, S.D. = 10.94%). Applying similar inclusion
229 criteria, we identified 2,330 autosomal, post-QC CpG sites previously associated with former
230 smoking² (hereafter called the “former-smoking-associated CpGs”), which were analyzed in the
231 MR-DoC1 models for *Former Smoking* → *DNAm*. A subset of 1,782 (76.5%) former-smoking-
232 associated CpGs had mQTL allelic scores with F-statistic >10 and were examined in the MR-
233 DoC1 models for *DNAm* → *Former Smoking* and the bidirectional models.

234

235 We used a PRS of lifetime regular-smoking initiation²⁰ as the IV for smoking status, which had
236 an incremental liability-scale R² of 5.07% (F-statistic = 73.2) for current versus never smoking
237 and 2.02% (F-statistic = 28.8) for former versus never smoking in the target NTR dataset.

238

Causation between Smoking and DNA methylation



239

240 **Figure 2. Selection of CpG sites tested in each MR-DoC model.**

241 *Previous independent EWAS meta-analysis of cigarette smoking² examined DNA methylation*
242 *(DNAm) at CpG sites from the Illumina HumanMethylation450 BeadChip array²¹, which was*

Causation between Smoking and DNA methylation

243 *also used to measure DNAm in the NTR biobank. In the unidirectional MR-DoC1 models for*
244 *Smoking → DNAm, we included autosomal CpG sites associated with smoking in the EWAS*
245 *meta-analysis that also passed the QC metrics in NTR. The MR-DoC1 models for DNAm →*
246 *Smoking and the bidirectional MR-DoC2 models were restricted to a subset of these sites having*
247 *cis-mQTL summary statistics from the GoDMC¹⁸ and a resulting mQTL allelic score with F-*
248 *statistic >10.*
249

250 **Exemplar: Putative causality between current smoking and *AHRR* DNAm**

251 To illustrate the three MR-DoC models, we first present the results for two CpG sites
252 (cg23916896 and cg05575921) in the Aryl-Hydrocarbon Receptor Repressor (*AHRR*) gene,
253 which are among the most well-established DNAm signatures of cigarette smoking².

254
255 One of the two MR-DoC1 model specifications allowed us to estimate and account for potential
256 unbalanced horizontal pleiotropy from the mQTL allelic score to smoking in *DNAm* → *Smoking*
257 models and from the smoking PRS to DNAm in *Smoking* → *DNAm* models. However, to
258 estimate this pleiotropic association, the model requires fixing the confounding due to unique
259 environmental factors to a specific value (here, zero)¹³. In the second specification of MR-DoC1,
260 we freely estimated and controlled for potential unique environmental confounding (labeled “rE”
261 in Figure 1), while instead assuming that the IV had no horizontal pleiotropy. In MR-DoC2
262 models, we estimated bidirectional causal effects by including both the smoking PRS and the
263 mQTL allelic score, while allowing the two IVs to covary with each other¹⁴. Covariance between
264 the PRS and the mQTL allelic score may arise from many possible sources, including shared
265 pleiotropic SNPs, LD between the constituent SNPs, and population structure. Therefore, MR-
266 DoC2 may help reduce potential biases in the causal estimates by accounting for these sources of
267 covariance between smoking PRS and mQTL allelic score. Across all models, causal
268 relationships with the binary smoking variable are estimated on the latent liability scale²². So,
269 even where smoking is the “exposure” variable, the causal estimate is interpreted as the effect of
270 the underlying smoking *liability* rather than smoking *exposure*.

271
272 For probe cg23916896 (**Figure 3A**), the mQTL allelic score had an incremental R² of 8.03% (F-
273 statistic = 156.4). The estimated effects indicated that higher liability for current smoking likely
274 causes hypomethylation of cg23916896, with consistently negative causal estimates: -0.82 (95%
275 confidence interval: -1.20, -0.44) in MR-DoC1 with horizontal pleiotropy, -0.43 (-0.62, -0.24) in
276 MR-DoC1 with unique environmental confounding, and -0.38 (-0.55, -0.21) in the bidirectional
277 MR-DoC2 model. These estimates remained statistically significant after FDR correction in all
278 three models. The estimated reverse effect of cg23916896 methylation on the liability for current
279 smoking also had consistently negative estimates in all models: -0.24 (-0.37, -0.12) in MR-DoC1
280 with horizontal pleiotropy, -0.32 (-0.61, -0.04) in MR-DoC1 with unique environmental
281 confounding, and -0.32 (-0.61, -0.04) in MR-DoC2. That is, hypomethylation of cg23916896
282 putatively increases the liability for current smoking. These estimates were statistically
283 significant at false discovery rate (FDR) <0.05 in MR-DoC1 with horizontal pleiotropy, but only
284 nominally significant (p <0.05) in the other two models. Taken together, these results provide
285 robust evidence for current smoking’s causal effects on cg23916896 methylation, with
286 suggestive evidence for the reverse effect of cg23916896 methylation on smoking. Previous MR
287 studies of lifetime smoking and DNAm have not examined this CpG site, as these studies
288 focused on a few selected sites^{10,11}. Our analyses indicate that cg23916896 potentially has a

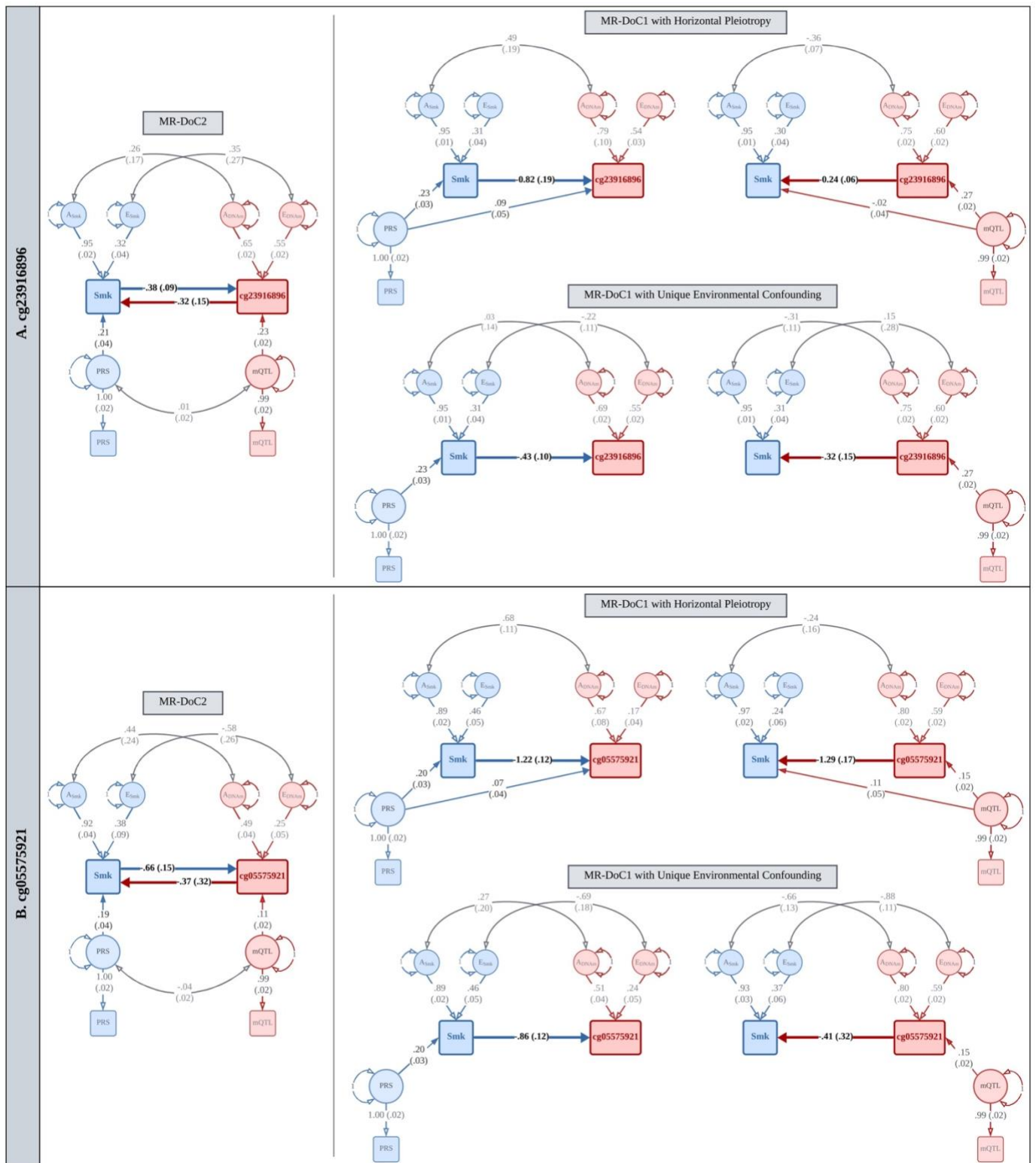
Causation between Smoking and DNA methylation

289 bidirectional causal relationship with cigarette smoking, such that the smoking-induced
290 hypomethylation at this locus may reciprocally increase the liability for smoking.

291
292 In comparison, probe cg05575921 (one of the CpGs most robustly associated with cigarette
293 smoking) had an mQTL allelic score with a relatively modest incremental R^2 of 1.74% (F-
294 statistic = 31.6). Similar to cg23916896, the effect of current smoking liability on cg05575921
295 methylation had consistently negative, robust estimates, with FDR <0.05 in all three models
296 (**Figure 3B**), which also aligns with the previously reported negative, albeit non-significant,
297 effect of *lifetime* smoking¹⁰. The reverse effect of cg05575921 methylation on smoking liability
298 was estimated to be -1.29 (-1.62, -0.96) in MR-DoC1 with horizontal pleiotropy, -0.41 (-1.03,
299 0.21) in MR-DoC1 with unique environmental confounding, and -0.37 (-1.00, 0.26) in MR-
300 DoC2. Although the point estimates were negative in all three models, they were not statistically
301 significant in the latter two models. Notably, the point estimates for cg05575921 are comparable
302 to those for cg23916896 but have larger standard errors, likely due to the former's weaker IV
303 (mQTL allelic score).

304

Causation between Smoking and DNA methylation



305
 306 **Figure 3. Illustrative MR-DoC models of causality between current smoking and blood DNAm**
 307 **at (A) cg23916896 and (B) cg05575921 in the AHRR gene.**

Causation between Smoking and DNA methylation

308 *We fitted five MR-DoC models at each CpG: (1) Smoking \rightarrow DNAm MR-DoC1 with horizontal*
309 *pleiotropy, (2) Smoking \rightarrow DNAm MR-DoC1 with unique environmental confounding, (3) DNAm*
310 *\rightarrow Smoking MR-DoC1 with horizontal pleiotropy, (4) DNAm \rightarrow Smoking MR-DoC1 with unique*
311 *environmental confounding, and (5) bidirectional MR-DoC2. Thus, for each CpG, three causal*
312 *estimates were obtained in either direction of causation.*

313 *In the path diagrams, squares/rectangles indicate observed variables, circles indicate latent*
314 *(unobserved variables), single-headed arrows indicate regression paths, and double-headed*
315 *curved arrows indicate (co-)variance. The residual variance of smoking status liability is*
316 *partitioned into additive genetic (A_{Smk}) and unique environmental (E_{Smk}) components. Likewise,*
317 *the residual variance of DNAm is partitioned into A_{DNAm} and E_{DNAm} . The correlation between*
318 *A_{Smk} and A_{DNAm} represents the confounding between smoking and DNAm due to latent*
319 *(unobserved) additive genetic factors, while the correlation between E_{Smk} and E_{DNAm} represents*
320 *confounding due to latent unique environmental factors. Each model included age and sex as*
321 *covariates of smoking status (not shown). DNAm β -values were residualized for standard*
322 *biological and technical covariates used in EWAS (see Methods). The smoking PRS and the*
323 *mQTL allelic scores were residualized for standard GWAS covariates, including genetic*
324 *principal components and genotyping platform. In the path diagrams, the residualized PRS and*
325 *mQTL allelic scores are regressed on respective latent factors, representing the underlying*
326 *“true” standardized scores (mean = zero; variance = one). The coefficient of the path from the*
327 *latent score to the observed score estimates the standard deviation of the observed score.*
328 *Note. The paths are labeled by the point estimate and its S.E. in parentheses. For better*
329 *readability, the path diagrams show only the within-individual part of the models fitted to data*
330 *from twin pairs.*
331

332 **Evidence of more widespread effects of current smoking on DNAm than *vice*** 333 ***versa***

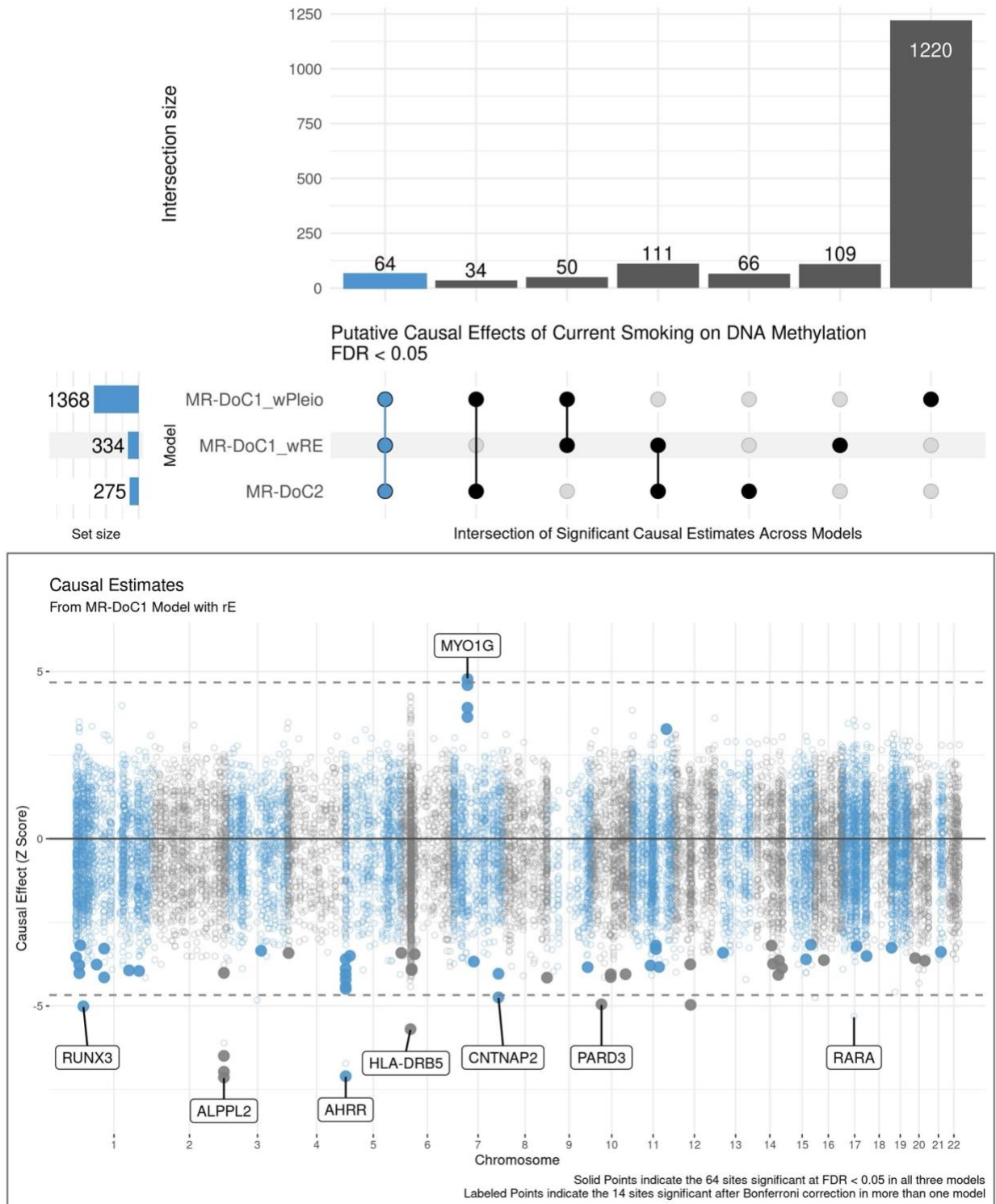
334 To evaluate whether there was evidence of widespread, small causal effects of current smoking
335 on DNAm, we examined the Bayesian genomic inflation factor²³ (λ) using p-values of the causal
336 estimates. Across the 16,940 smoking-associated CpG sites, MR-DoC1 with horizontal
337 pleiotropy had $\lambda = 1.44$, while MR-DoC1 with unique environmental confounding showed $\lambda =$
338 1.20. For comparison, fitting similar models epigenome-wide at 411,169 autosomal, post-QC
339 CpGs showed much less inflation ($\lambda = 0.98$ and $\lambda = 1.09$, respectively), suggesting enrichment of
340 low p-values among the smoking-associated CpGs. The epigenome-wide inflation is in line with
341 that for cigarettes per day ($\lambda > 1.1$) previously reported using two-sample MR¹⁸. Corresponding
342 QQ plots showed a deviation of the causal estimate p-values from the null hypothesis across a
343 broad range of smoking-associated CpG sites (**Supplementary Figures S1, S2**). Across the
344 11,124 CpG sites with bidirectional MR-DoC2 models, the estimated reverse effects of DNAm
345 on current smoking showed little inflation ($\lambda = 1.01$) compared to the effects of current smoking
346 on DNAm in the same model ($\lambda = 1.20$; **Supplementary Figures S3, S4**). These findings
347 suggest that the causal influences of current smoking on DNAm likely contribute, at least partly,
348 to the previously reported EWAS hits. For the reverse effects of DNAm on current smoking, the
349 absence of λ inflation does not preclude potential localized small effects at several CpG sites.
350 Furthermore, despite the inflation of the test statistics, our sample size might be insufficient to
351 obtain significant estimates of relatively small effects in either direction of causation.

352
353 There also was considerable variability in the number of CpG sites with statistically significant
354 causal estimates across models. The estimated *Current Smoking* \rightarrow *DNAm* effects had FDR
355 < 0.05 at 1,368 CpGs in MR-DoC1 with horizontal pleiotropy, 334 CpGs in MR-DoC1 with
356 unique environmental confounding, and 275 CpGs in MR-DoC2 (**Figure 4; top panel**). The
357 relatively higher number of statistically significant causal estimates in MR-DoC1 with horizontal
358 pleiotropy may partly be due to its higher power compared to the other models²⁴. Looking at the
359 intersection of significant estimates across models, 259 CpG sites showed FDR < 0.05 in at least
360 two models, while 64 sites showed FDR < 0.05 in all three models. These 64 sites also showed
361 consistency in the direction of effect across all three models (**Supplementary Figure S5, Table**
362 **S1**). Thus, we considered these 64 CpG sites to exhibit robust evidence for the causal effects of
363 current smoking liability on DNAm, including hypomethylation of 59 sites and hypermethylation
364 of the other five (**Figure 4; bottom panel**). These CpGs are annotated to some of the top genes
365 implicated in prior EWAS of smoking², including hypomethylation of CpGs in/near *AHRR*,
366 *ALPPL2* (alkaline phosphatase placental-like 2), *CNTNAP2* (contactin-associated protein 2), and
367 *PARD3* (par-3 family cell polarity regulator) and hypermethylation of CpGs in *MYO1G* (myosin
368 1G). Only one of these 64 CpG sites lies within the major histocompatibility complex (MHC)
369 region (chr6:28477797-33448354): cg06126421 located near gene *HLA-DRB5*. Due to its
370 complex LD structure, the causal estimates of the sites in the MHC region should be interpreted
371 with caution.

Causation between Smoking and DNA methylation

372

Putative Causal Effects of Current Smoking on DNA Methylation in MR-DoC Models



373

374

Causation between Smoking and DNA methylation

375 **Figure 4. Putative Causal Effects of Current Smoking on Blood DNA Methylation in MR-**
376 **DoC Models**

377 *The top panel shows an UpSet plot of the intersection of CpG sites with statistically significant*
378 *(FDR <0.05) estimates of Current Smoking → DNAm in the three MR-DoC models. The matrix*
379 *consists of the models along the three rows and their intersections along the columns. The*
380 *horizontal bars on the left represent the number of CpGs with significant (FDR <0.05) causal*
381 *estimates in each model. The vertical bars represent the number of CpGs belonging to the*
382 *respective intersection in the matrix.*

383 *The bottom panel shows a Miami plot of the Current Smoking → DNAm causal estimates across*
384 *16,940 smoking-associated CpGs. The X-axis shows the genomic positions of the CpG sites*
385 *aligned to Genome Reference Consortium Human Build 37 (GRCh37). The Y-axis shows the Z-*
386 *statistic of the estimated effect of the liability for current (versus never) smoking on (residualized*
387 *and standardized) DNA methylation β -values in the MR-DoC1 model with unique environmental*
388 *confounding (rE). The solid points indicate the 64 sites with significant causal estimates (FDR*
389 *<0.05) in all three models (i.e., the blue vertical bar in the UpSet plot). The CpG sites with*
390 *causal estimates significant after Bonferroni correction in more than one model are labeled by*
391 *their respective nearest gene.*

392 *Note. The data underlying these plots are in **Supplementary Table S1**.*

393

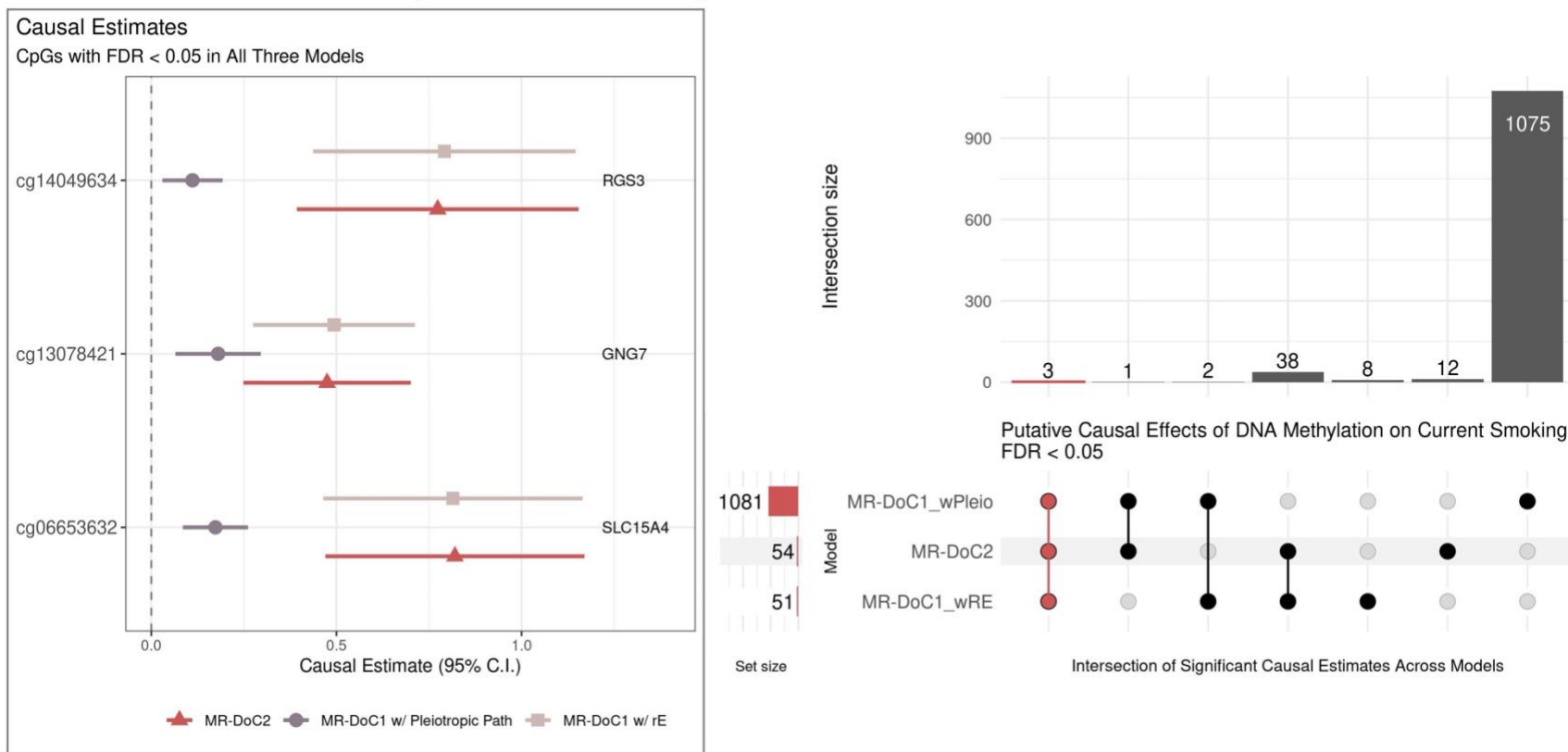
Causation between Smoking and DNA methylation

394 On applying a more conservative Bonferroni correction for multiple testing, 14 sites had
395 significant *Current Smoking* → *DNAm* causal estimates in more than one model, while only four
396 CpGs had significant estimates in all three models (**Supplementary Figure S6**). Thus, these four
397 CpGs showed the most robust evidence for the effects of current smoking on DNAm, comprising
398 three sites with hypomethylation (cg05951221 and cg01940273 near *ALPPL2*, and cg06126421
399 near *HLA-DRB5*) and one with hypermethylation (cg12803068 in *MYO1G*).

400
401 The estimated *DNAm* → *Current Smoking* effects were significant (FDR <0.05) at 1,081 CpGs
402 in MR-DoC1 with horizontal pleiotropy, 51 CpGs in MR-DoC1 with unique environmental
403 confounding, and 54 CpGs in MR-DoC2 (**Figure 5; right panel**). Further, 44 CpGs showed
404 FDR <0.05 in at least two models, but only three CpGs had FDR <0.05 in all three models. The
405 three CpGs also had consistent, positive estimates across models, suggesting that
406 hypermethylation of CpG sites in *GNG7* (G-Protein Subunit Gamma 7), *RGS3* (Regulator of G-
407 Protein Signaling 3), and *SLC15A4* (Solute Carrier Family 15 Member 4) genes may increase the
408 liability for current smoking (**Figure 5; left panel**). None of these sites has been previously
409 reported to have effects on smoking liability¹¹. Applying the more conservative Bonferroni
410 correction, nine CpGs had significant *DNAm* → *Current Smoking* causal estimates in more than
411 one model, but none showed Bonferroni-corrected significant effects in all three models
412 (**Supplementary Figure S7**).

413

Putative Causal Effects of DNA Methylation on Current Smoking in MR-DoC Models



414

415 **Figure 5. Putative causal effects of blood DNA methylation on current-smoking liability in MR-DoC models**

416 The left panel shows the estimates and Wald-type 95% confidence intervals of the causal effects of (residualized and standardized)
 417 DNA methylation β -values on the liability for current (versus never) smoking in each of the three MR-DoC models: bidirectional MR-
 418 DoC2, MR-DoC1 with horizontal pleiotropic path, and MR-DoC1 with unique environmental confounding (rE). The text labels
 419 indicate the gene to which the CpG is annotated.

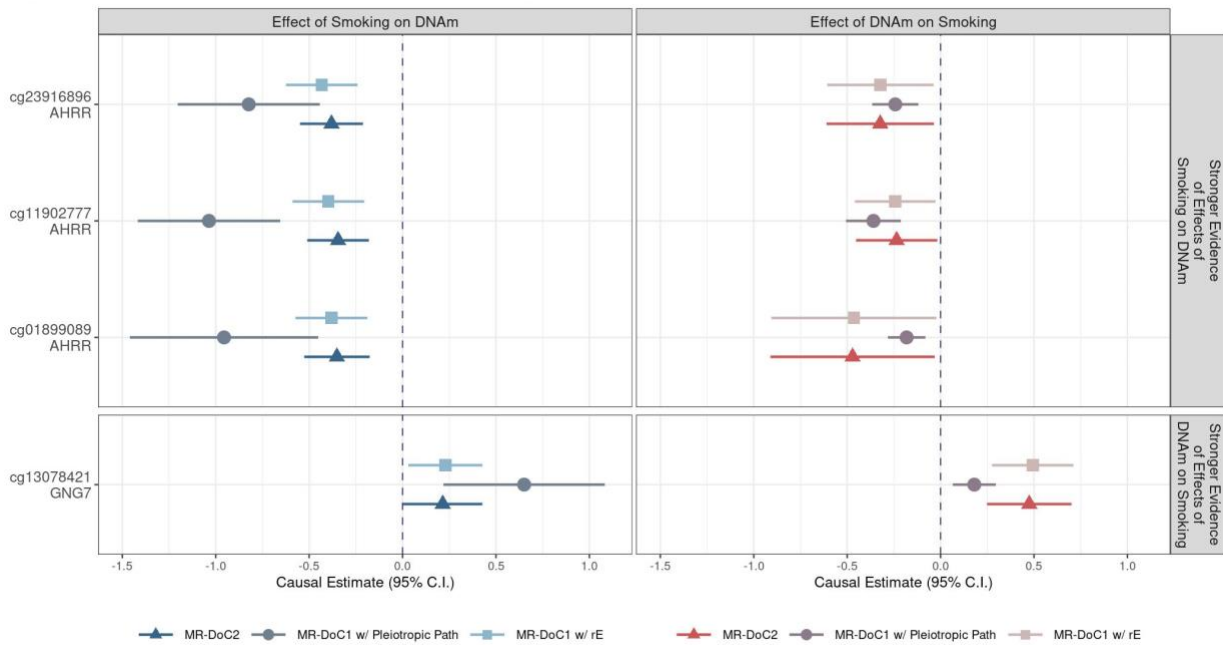
420 *The right panel shows an UpSet plot of the intersection of CpG sites with statistically significant ($FDR < 0.05$) estimates of DNAm →*
421 *Current Smoking in each of the three MR-DoC models. The matrix consists of the models along the three rows and their intersections*
422 *along the columns. The horizontal bars on the left represent the number of CpGs with significant ($FDR < 0.05$) causal estimates in*
423 *each model. The vertical bars represent the number of CpGs belonging to the respective intersection in the matrix.*
424 *Note. The data underlying these plots are in **Supplementary Table S3**.*
425

Causation between Smoking and DNA methylation

426 **Suggestive Evidence of Bidirectional Effects at Four CpG Sites**

427 The 64 CpG sites with robust evidence of current smoking’s effects on DNAm do not overlap
 428 with the three sites with robust evidence of reverse effects. However, further examining the
 429 causal estimates revealed that three of the 64 sites also had consistently negative, nominally
 430 significant ($p < 0.05$) estimates of $DNAm \rightarrow Current\ Smoking$ effects in all models (**Figure 6**).
 431 The three CpGs (cg23916896, cg11902777, cg01899089) are all located in the *AHRR* gene,
 432 suggesting potential bidirectional effects between current smoking and *AHRR* DNAm. That is,
 433 current smoking putatively causes hypomethylation of CpGs in *AHRR*, which, in turn, may
 434 further increase smoking liability as a feedback effect. Among the CpGs with robust evidence of
 435 DNAm’s effects on current smoking, cg13078421 (*GNG7*) also showed consistently positive,
 436 nominally significant estimates of current smoking’s effects on DNAm. Thus, *GNG7*
 437 hypermethylation putatively increases smoking liability, with a potential reverse effect of current
 438 smoking on *GNG7* methylation. Additionally, 15 CpGs had consistent, nominally significant
 439 bidirectional causal estimates in all three models, though the estimates were not significant after
 440 FDR correction in either direction (**Supplementary Figure S8**).
 441

Suggestive Bidirectional Causal Effects between Current Smoking and Blood DNA Methylation



442

443 **Figure 6. Potential bidirectional effects between current smoking and blood DNA methylation**

444 *Estimates and Wald-type 95% confidence intervals of bidirectional causal effects between the*
 445 *liability for current (versus never) smoking and (residualized and standardized) DNA*
 446 *methylation β -values in the three MR-DoC models: bidirectional MR-DoC2, MR-DoC1 with*
 447 *horizontal pleiotropic path, and MR-DoC1 with unique environmental confounding (rE). The Y-*

Causation between Smoking and DNA methylation

448 *axis labels indicate the CpG probe IDs and the respective genes in which the CpGs are located.*
449 *Three of the four CpGs are in the AHRR gene and show robust evidence of the causal effects of*
450 *current smoking on DNAm, along with weaker evidence of the reverse effects of DNAm on*
451 *smoking. On the other hand, the fourth CpG is located in the GNG7 gene and shows robust*
452 *evidence of the causal effects of DNAm on current smoking, with weaker evidence of the reverse*
453 *effects of smoking on DNAm.*
454 *Note. The data underlying these plots are in **Supplementary Tables S1-S4.***
455

456 **DNAm loci potentially influenced by smoking are enriched for biological**
457 **processes relevant to smoking's adverse health outcomes**

458 For follow-up gene-set annotation and functional enrichment analyses²⁵, we identified 525 CpG
459 sites (outside the MHC region) with potential effects of current smoking on DNAm based on
460 consistent, nominally significant estimates in all three models (**Supplementary Table S1**). The
461 genes mapped by these CpGs showed extensive significant enrichment (FDR <0.05) for ontology
462 clusters, including hemopoiesis, cell morphogenesis, inflammatory response, regulation of cell
463 differentiation, and regulation of nervous system development, underscoring DNAm's potential
464 role in the adverse health sequelae of smoking (**Supplementary Figures S9-S11; Tables S5-S6**).

465
466 Next, we performed *eFORGE 2.0* (experimentally derived Functional element Overlap analysis
467 of ReGions from EWAS)^{26,27} analyses to explore the tissue-specific functional relevance of these
468 CpG sites. These sites were significantly enriched (FDR <0.05) for overlap with a wide range of
469 gene regulatory elements, including chromatin states, histone marks, and DNase-I hotspots, in
470 most of the tissue/cell types in reference datasets. These findings suggest that the functional
471 consequences of the effects of smoking on DNAm are likely widespread across the body rather
472 than specific to a few tissue types (**Supplementary Figures S12-S14; Tables S7-S9**).

473 **CpG sites with consistent effects on current smoking show enrichment for**
474 **brain-related gene regulatory elements**

475 For potential *DNAm* → *Current Smoking* effects, we identified 64 CpGs with consistent,
476 nominally significant estimates in all three models (**Supplementary Figure S15**). In the gene-set
477 enrichment analyses (**Supplementary Figures S16-S17; Tables S10-S11**), the genes mapped by
478 these CpGs did not show significant functional enrichment (FDR <0.05), likely due to too few
479 loci implicated in this direction of causation. However, in the *eFORGE* analyses, which use
480 precise chromatin-based information for each CpG, these CpG sites showed significant
481 enrichment (FDR <0.05) for overlap with enhancers in the brain (fetal brain), blood (primary B
482 cells, hematopoietic stem cells), lung, and mesodermal embryonic stem cells (**Supplementary**
483 **Figures S18-S20; Tables S12-S14**). This set of CpGs also showed significant enrichment for
484 histone marks in multiple tissues/cell types (including the brain, blood, and lung), but the overlap
485 with DNase-I hotspots was not significantly enriched. The tissues/cell types predicted to be
486 relevant for DNAm's effects on smoking liability may be prioritized for follow-up tissue-/cell
487 type-specific studies.

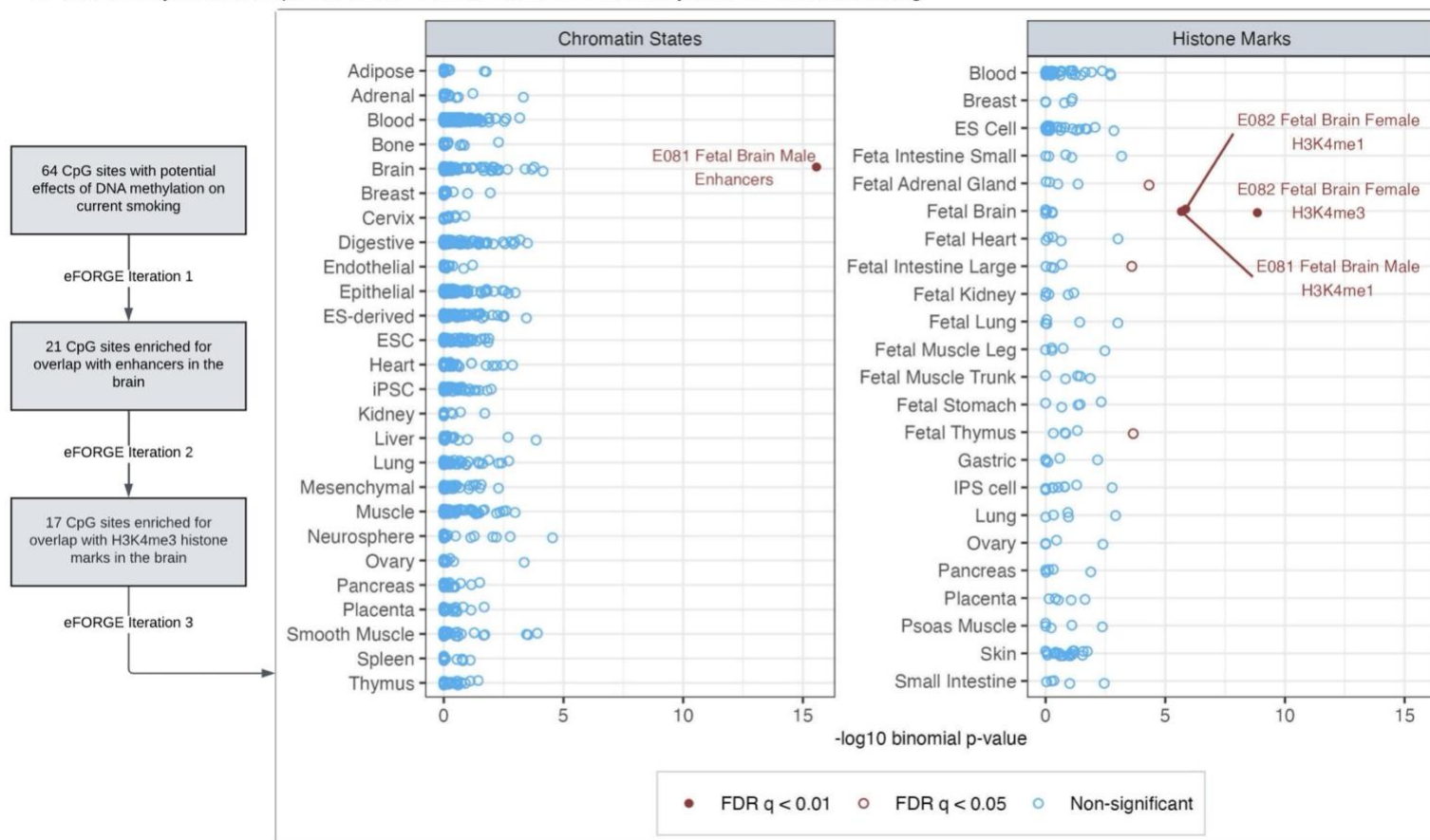
488
489 To further gauge the tissue-specificity of the *eFORGE* enrichment, we performed iterative
490 follow-up analyses with the CpGs overlapping with tissue/cell types of interest (see **Methods**
491 and **Supplementary Figures S21-S23; Tables S15-S17**). These analyses elucidated a subset of
492 17 CpGs with significant and highly specific enrichment for enhancers and histone marks
493 (H3K4me1 and H3K4me4) in the brain (**Figure 7**), along with weaker enrichment for H3K4me1

Causation between Smoking and DNA methylation

494 in the adrenal gland and thymus. Ten of the 17 sites also overlapped with DNase-I hotspots in the
495 brain, though the enrichment was not statistically significant (FDR = 0.08) (**Supplementary**
496 **Figure S24, Table S20**). The causal estimates and the nearest gene of these 17 CpGs are shown
497 in **Supplementary Figure S25**. Four of these CpGs also had consistent estimates of the reverse
498 effects of current smoking on DNAm (identified by the column “g1_nominal” in
499 **Supplementary Table S4**): cg25612391 (*SLC25A42*), cg05424060 (*GNAII*), cg10590964 (near
500 *KIAA2012*), and cg05877788 (*TP53II3*). Furthermore, prior pre-clinical and clinical studies have
501 implicated 14 of the 17 mapped genes, including three with potential bidirectional effects, in
502 behavioral or neurological traits, such as alcohol dependence (*OSBPL5*)²⁸, cocaine use
503 (*SLCO5A1*)²⁹, anxiety (*CCDC92*)³⁰, depression (*GNAII*)³¹, encephalomyopathy and brain stress
504 response (*SLC25A42*)^{32,33}, and dementia or Alzheimer’s disease pathology (*SIAH3*, *SRM*,
505 *TP53II3*)^{34–36}.

506
507 Similar follow-up analyses with other subsets of CpGs (e.g., probe sets enriched for enhancers in
508 the lung or cord blood primary B cells) showed enrichment across several tissue/cell types,
509 suggesting non-specificity of the enrichment seen in these tissues (**Supplementary Figures S26-**
510 **S31; Tables S21-S26**). The enrichment for specific blood cell types (here, B cells) may be partly
511 confounded by residual cell-composition effects in whole blood analyses²⁶. The 18 CpGs
512 overlapping with enhancers in primary B cells mapped to 16 genes, of which five have been
513 previously associated with (any) blood cell counts but only one with lymphocyte count in
514 GWAS³⁷. Thus, the sites driving the enrichment for B cells had little overlap with the known
515 lymphocyte-count GWAS associations. For comparison, the 64 CpGs with potential *DNAm* →
516 *Current Smoking* effects annotated to 51 genes, of which 16 are known to be associated with
517 (any) blood cell counts and only two with lymphocyte count.

eFORGE Analyses of the CpG Sites with Potential Effects of DNA Methylation on Current Smoking



518

519 **Figure 7. Among the CpG sites with potential effects of blood DNA methylation on current smoking liability, iterative eFORGE**
 520 **analyses elucidated sites enriched for overlap with brain-related chromatin states and histone marks.**

521 *The first iteration of eFORGE examined the 64 CpG sites with potential effects of blood DNA methylation on current smoking liability*
 522 *(Supplementary Figure S15), revealing 21 CpGs enriched for overlap with enhancers in the brain (Supplementary Figure S18/Table*
 523 *S12). In follow-up analyses restricted to these 21 CpGs (eFORGE iteration 2), all 21 probes were also enriched for the brain*

524 *H3K4me1* marks, while 17 of these probes overlapped with *H3K4me3* marks in the brain (Supplementary Figure S22/Table S16). This
525 iteration also showed significant enrichment ($FDR\ q < 0.01$) for histone marks in other tissues, including small and large intestines,
526 adrenal gland, and thymus. So, to identify a subset of these CpGs with potentially more specific enrichment for brain-related
527 functional elements, we restricted further analyses to the 17 sites overlapping with the brain *H3K4me3* marks (eFORGE iteration 3).
528 As seen in this figure, these 17 sites showed highly specific enrichment for enhancers and histone marks in the brain (**Supplementary**
529 **Tables S18-S19**). Ten of these sites also overlapped with DNase-I hotspots in the brain (Supplementary Table S20).

530 **Attenuated effects of former smoking on DNAm**

531 MR-DoC analyses estimating the causal effects between former smoking and DNAm showed
532 attenuated inflation factor (λ) in all models, compared to the λ values in similar models fitted to
533 current smoking. For instance, the MR-DoC2 models fitted across the 11,124 smoking-
534 associated CpGs had $\lambda = 1.11$ for *Former Smoking* \rightarrow *DNAm* and $\lambda = 0.99$ for *DNAm* \rightarrow *Former*
535 *Smoking*, compared to 1.20 and 1.01, respectively, for current smoking. Note that these λ
536 calculations were not restricted to the former-smoking-associated CpGs to allow for a
537 comparison with current smoking.

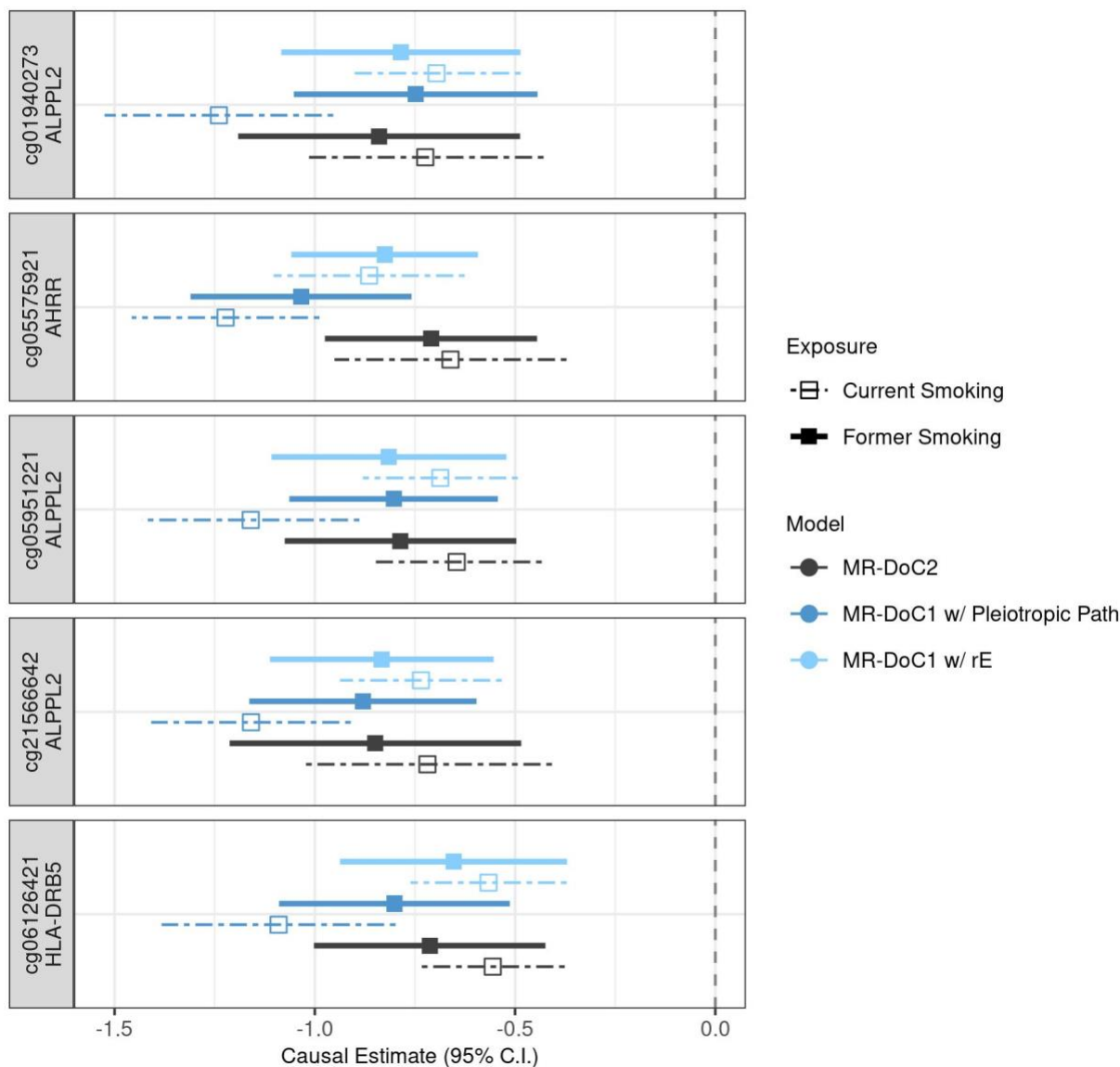
538
539 Among the former-smoking-associated CpGs, only five sites showed robust evidence of causal
540 effects of former smoking on DNAm, with consistent, statistically significant (FDR <0.05)
541 causal estimates in all three models (**Supplementary Figure S32**). These CpGs include
542 cg05575921 in *AHRR*, cg05951221, cg01940273, and cg21566642 near *ALPPL2*, and
543 cg06126421 near *HLA-DRB5* gene (in the MHC region). The causal estimates at these sites are
544 similar to those of the effects of current smoking on DNAm, with overlapping confidence
545 intervals (**Figure 8**). Thus, unlike most smoking-associated CpGs³⁸, smoking's effects on DNAm
546 at these sites likely have limited reversibility, in line with the previously reported persistent
547 associations of these sites with former smoking 30 years after cessation². For the reverse effects
548 of DNAm on former smoking, no CpG showed consistent (at least nominally significant) causal
549 estimates across models (**Supplementary Figure S33**). Nevertheless, of the three CpGs with
550 robust evidence of DNAm's effects on current smoking, two were among the former-smoking-
551 associated CpGs and had overlapping confidence intervals of the estimated effects of DNAm on
552 *former* smoking and *current* smoking (**Supplementary Figure S34**).

553

Causation between Smoking and DNA methylation

CpGs with Putative Effects of Former Smoking on DNA Methylation

Sites with FDR < 0.05 in All Three Models



554

555 **Figure 8. Putative causal effects of former smoking on blood DNA methylation.**

556 *Estimates and Wald-type 95% confidence intervals of the causal effects of the liability for former*
 557 *(versus never) smoking and (residualized and standardized) DNA methylation beta-values in*
 558 *each of the three MR-DoC models: bidirectional MR-DoC2, MR-DoC1 with horizontal*
 559 *pleiotropic path, and MR-DoC1 with unique environmental confounding (rE). The*
 560 *corresponding estimates for current (versus never) smoking are also shown with dashed lines.*
 561 *The text labels on the left indicate the CpG probe IDs and the genes mapped by the CpGs.*
 562 *Note. The data underlying these plots are in **Supplementary Tables S1 and S27**, indicated by the*
 563 *column `gl_robust`.*

564

565

Discussion

566 Results from integrated MR and biometrical genetic (MR-DoC) modeling suggest that the causal
567 effects of cigarette smoking on blood DNAm likely underlie many of the associations seen in
568 EWAS. Compared to a handful of CpGs previously found to be causally linked with smoking in
569 standard MR studies, we found over 500 CpGs with consistent, nominally significant effects of
570 current smoking on DNAm. These CpGs show broad enrichment for tissue types and functional
571 pathways that implicate numerous well-established harmful health outcomes of smoking,
572 including cell- and neuro-development, carcinogenesis, and immune regulation. In the analyses
573 of former smoking, most of the estimated effects of smoking on DNAm were no longer
574 significant, consistent with the reversibility of smoking's effects at these loci. Additionally,
575 several CpG sites showed evidence of reverse and possibly bidirectional effects of DNAm on the
576 liability for current smoking, with a subset of these loci enriched for gene regulatory functional
577 elements in the brain. The detection of reverse or bidirectional causal effects of blood DNAm on
578 smoking highlights the potential utility of blood DNAm as a putative biomarker to monitor
579 addiction or interventions.

580

581 Previous analyses of smoking-discordant twin pairs in NTR, a subset of the current study sample,
582 found 13 CpG sites with significant DNAm differences between MZ twins discordant for current
583 smoking³⁹, suggesting potential causality. In our MR-DoC analyses, eight of the 13 CpGs
584 showed robust evidence of causal effects of current smoking on DNAm, while none showed
585 reverse effects. Taken together, the findings from the two studies further triangulate the evidence
586 for smoking's effects on DNAm at these sites. Prior summary-statistics-based MR studies have
587 examined causality between *lifetime* (current or former) cigarette smoking and blood DNAm.
588 The MR analyses in GoDMC¹⁸ did not find evidence of causal effects of lifetime smoking on
589 DNAm, nor *vice versa*. Another study¹⁰ applied a single MR method and found nominally
590 significant effects of lifetime smoking on DNAm at 11 CpG sites from the Illumina
591 MethylationEPIC array⁴⁰, of which two (cg14580211, cg15212295) overlap with Illumina 450k
592 array data used in the current study. In our MR-DoC analyses, only cg14580211 showed
593 replication in the form of consistent negative causal estimates of current smoking on DNAm.
594 The novel and more extensive causal effects found in our analyses may partly be attributable to
595 the study design's ability to estimate the causal influences of *current* smoking specifically, as
596 most smoking-associated DNAm changes exhibit substantial reversibility upon smoking
597 cessation^{2,21}. Furthermore, the nine CpGs with previously reported reverse effects of DNAm on
598 lifetime smoking behavior (a composite index of initiation, heaviness, and cessation)¹¹ in a single
599 MR model showed inconsistent estimates in the three MR-DoC models. Interestingly, two of
600 these CpGs (cg09099830 and cg24033122; both located in gene *ITGAL*) instead showed
601 consistent, nominally significant effects of current smoking on DNAm, underscoring the need for
602 further replication of both prior and current findings.

603

Causation between Smoking and DNA methylation

604 Of the three CpG sites with robust evidence of DNAm's effects on current smoking liability, two
605 are located in genes *GNG7* and *RGS3* that are integral to G protein-coupled receptor (GPCR)
606 signaling, adding to the growing literature on GPCR signaling pathways' potential role in
607 behavioral and neuropsychiatric outcomes⁴¹. Specifically, differential expressions of both
608 *GNG7*⁴² and *RGS3*⁴³ have been associated with addiction-related phenotypes in model
609 organisms. The third CpG annotates to *SLC15A4*, which encodes a lysosomal peptide/histidine
610 transporter involved in antigen presentation and innate immune response⁴⁴, including in mast
611 cells⁴⁵. Thus, DNAm variation at this locus may plausibly reflect individual differences in
612 immunological tolerance of cigarette smoke and, consequently, maintenance of smoking
613 behavior. Interestingly, these CpGs were significantly associated with neither cannabis use⁷ nor
614 alcohol consumption⁶ in recent large-scale EWASs. Notably, though, both these studies reported
615 DNAm associations conditional on cigarette smoking, making them unsuitable for gauging
616 whether the CpGs with putative effects on smoking liability are also associated with other
617 substances. This raises the question of whether cigarette smoking should always be used as a
618 covariate in EWAS. If so, it may be prudent to report supplementary EWAS results without
619 smoking as a covariate, as some CpGs may have a reverse or bidirectional causal relationship
620 with smoking. Note that the EWAS of cannabis use⁷ did perform such preliminary analyses but
621 only reported the results conditional on cigarette smoking.

622
623 Several factors need to be considered when interpreting the above results. Although we found
624 relatively few sites with putative effects of whole blood DNAm on smoking liability or with
625 suggestive bidirectional effects, the situation might differ in specific blood cell types or other
626 tissues relevant to smoking, like the brain. The results may also vary in other peripheral tissues,
627 like buccal cells⁴⁶. Moreover, the highly variable predictive strength of mQTL allelic scores
628 across CpG sites (incremental- R^2 range: 0.43-76.95%; median 4.61%) likely also influenced the
629 power to detect true causal effects of blood DNAm on smoking liability²⁴. When considering
630 similar model applications across different health traits, this impact on power is relevant to both
631 directions of causation, as the IV of other traits may not be as strong as the smoking PRS.
632 Additionally, the current study analyzed CpGs from the Illumina 450k array, which covers a
633 small fraction of genome-wide potential methylation sites. Further, many of the measured
634 smoking-associated CpGs lacked a "relevant" mQTL allelic score with F-statistic >10
635 (**Supplementary Figure S35**) and so are yet to be tested for *DNAm* → *Smoking* causal effects.
636 Newer low-cost sequencing technology⁴⁷ may help uncover more such causal relationships in the
637 future.

638
639 Like all MR studies, the current results depend on the validity of the IV assumptions¹⁹, which
640 cannot always be empirically tested. Here, we relied on the statistical significance and
641 consistency of the causal estimates across different specifications of MR-DoC models to account
642 for potential assumption violations, particularly horizontal pleiotropy. Yet, residual bias due to
643 violations of the assumptions underlying MR¹⁹ and biometrical twin modeling⁴⁸ cannot be ruled

Causation between Smoking and DNA methylation

644 out with certainty. Moreover, current MR-DoC models estimated linear causal effects. However,
645 since DNAm is constrained within certain biologically plausible values, the impact of smoking
646 on DNAm may depend on *prior* DNAm. To examine such non-linear causal relationships, MR-
647 DoC with interaction or quadratic effects would be a valuable area of further model
648 development, with numerous potential applications. Finally, we examined causality using only
649 binary smoking-status variables, as the sub-samples restricted to current or former smoking were
650 too small to fit MR-DoC models to smoking quantity (e.g., cigarettes per day) or time since
651 quitting. Further research with larger samples is needed to examine such dose-response causal
652 relationships.

653
654 The current study included participants of European ancestry only. Although prior EWASs show
655 highly concordant associations across ancestries^{2,7}, examining the generalizability of causal
656 estimates in non-European populations is a critical subject of further research. As MR-DoC
657 models provide causal inference specific to the target dataset, rather than the discovery GWAS
658 samples, future research may apply this study design to subpopulations of interest, e.g., stratified
659 by sex or age (such as children or elderly populations), provided the results from population-
660 wide GWAS generalize adequately. Future applications of MR-DoC analyses to DNAm data
661 may also extend the current work to other health traits and disorders that show robust
662 associations with DNAm and have strong genetic IVs. Recent developments in cost-effective
663 population-scale DNAm microarray technology⁴⁹ can help increase the sample sizes of twin
664 cohorts with DNAm data, enabling wider application of similar causal analyses.

665
666 In conclusion, the inability to establish causality is one of the key limitations of EWAS based on
667 surrogate tissues such as blood. Here, we demonstrate an application of the MR-DoC design to
668 examine causality between cigarette smoking and blood DNAm. The results suggest that many
669 of the EWAS associations are likely driven by the causal effects of current smoking on DNAm,
670 though we also find evidence of reverse and potentially bidirectional causal relationships at some
671 sites. Our study highlights the value of integrating DNAm, phenotypic information, and genetic
672 data in twin studies to uncover causal relationships of peripheral blood DNAm with human traits.
673 This study design might be valuable for detecting causal epigenetic biomarkers of (mental)
674 health in general.
675

676

Methods

677 Study Sample

678 The Netherlands Twin Register (NTR) is a community-based twin registry with longitudinal data
679 on health, behaviors, and lifestyle factors, combined with biological samples, including DNA
680 from blood and buccal samples. In the current analyses, we analyzed data from 2,577 individuals
681 participating in the NTR longitudinal surveys¹⁷ and the NTR biobank project⁵⁰. The study
682 participants comprised 1,730 (67%) female and 847 (33%) male individuals of European genetic
683 ancestry, including 706 monozygotic (MZ) twin pairs, 161 MZ individuals without their co-twin,
684 412 dizygotic (DZ) twin pairs, and 180 DZ individuals without their co-twin. The participants
685 had both genotypic and epigenome-wide DNAm data and were aged between 18 and 79 years
686 (mean 35.2; S.D. 11.7 years) at the time of blood sample collection.

687

688 Previous studies have described the NTR cohort in greater detail^{39,51}. NTR genotypic sample and
689 variant quality control (QC), imputation, genetic principal component analysis (PCA), and
690 ancestry-outlier pruning have been described previously⁵². Details specific to the participants
691 included in the present study are included in the **Supplementary Methods**. Since GoDMC¹⁸
692 summary statistics are available for European ancestry only, the current study sample excluded
693 109 participants identified as European-ancestry outliers in PCA to avoid bias due to ancestry
694 mismatch. The NTR is approved by the Central Ethics Committee on Research Involving Human
695 Subjects of the VU University Medical Centre, Amsterdam, an Institutional Review Board
696 certified by the U.S. Office of Human Research Protections (IRB number IRB00002991 under
697 Federal-wide Assurance- FWA00017598; IRB/institute codes, NTR 98-222, 2003-180, 2008-
698 244). All participants provided written informed consent before data collection.

699 Peripheral Blood DNA Methylation and Cell Counts

700 Epigenome-wide DNAm in peripheral whole blood was measured with the Infinium
701 HumanMethylation450 BeadChip Kit (i.e., the Illumina 450k microarray), following the
702 manufacturer's protocol²¹. QC and normalization of the DNAm data were performed using a
703 custom pipeline developed by the BIOS (Biobank-based Integrative Omics Study) Consortium,
704 as previously described⁵¹. Briefly, sample QC was done using MethylAid⁵³, followed by probe
705 QC with DNAmArray⁵⁴. The latter removed the probes with a raw signal intensity of zero, bead
706 number <3, or a detection p-value >0.01, as well as the ambiguously mapped probes. Next,
707 samples and probes with >5% missingness were removed. The resulting DNAm data were
708 normalized using the Functional normalization⁵⁵ algorithm implemented in DNAmArray⁵⁴, with
709 the first four PCs (with eigenvalue >1) derived from control probes. Finally, the probes
710 containing a SNP within the CpG site (at C or G nucleotide) were removed regardless of the
711 minor allele frequency. These SNPs were previously identified using DNA sequencing data from
712 the Dutch population⁵⁶. For the current analyses, only autosomal probes were included, yielding

Causation between Smoking and DNA methylation

713 411,169 CpG sites that passed all QC metrics, of which 16,940 sites were reported as associated
714 with current smoking (FDR <0.05) in an independent EWAS². Differential white blood cell
715 counts were also measured in the blood samples to estimate the proportions of neutrophils,
716 lymphocytes, monocytes, eosinophils, and basophils⁵¹.

717
718 Using linear regression models, the normalized β -values of DNAm at each CpG were corrected
719 for commonly used EWAS covariates⁵⁷, including age at blood draw, sex (genotypically inferred
720 biological sex, matched with self-reported gender), measured white blood cell percentages
721 (neutrophils, monocytes, and eosinophils) at blood draw, MH450k array row, and bisulfite
722 sample plate (dummy variables). The residuals from these regression models were standardized
723 (mean = 0, S.D. = 1) and used in MR-DoC models. As in the previous work in this dataset³⁹, we
724 did not include lymphocyte percentage as a regression covariate to prevent multicollinearity with
725 neutrophil percentage, while basophil percentage was not included because it had little variation
726 between individuals.

727 **Cigarette Smoking**

728 Self-reported cigarette smoking status was recorded through an interview during the home visit
729 for blood sample collection in 2004-2008 and 2010-2011. Participants were asked, “Do you
730 smoke?” with one of three possible answers: “No, I never smoked” (N = 1,492), “No, but I did in
731 the past” (N = 549), and “Yes” (N = 528). See **Supplementary Methods** for the original
732 wording in Dutch. Those endorsing current smoking were asked how many years they had been
733 smoking and how many cigarettes or rolling tobacco they smoked per day. Those endorsing
734 former smoking were asked how many years ago they quit smoking, how many years they had
735 smoked before quitting, and the maximum number of cigarettes or rolling tobacco they used to
736 smoke per day. The responses were checked for consistency with the information from the NTR
737 longitudinal surveys filled out closest to blood sampling. As previously described⁵⁸, potential
738 misclassification of smoking status through self-reports was evaluated based on plasma cotinine
739 levels (a metabolite of nicotine and a biomarker of smoking exposure), measured in a subset of
740 the sample. Of the 591 individuals with self-reported never smoking and measured plasma
741 cotinine, only five (0.8%) had cotinine levels indicative of smoking (≥ 15 ng/ml), thus suggesting
742 low misclassification of smoking status. The number of individuals endorsing current or former
743 smoking was too small to evaluate a dose-response relationship of the causal effects in MR-DoC
744 models restricted to currently or formerly smoking individuals. Likewise, the sample with former
745 smoking was too small to examine the effect of “time since quitting smoking” on DNAm.

746 **Instrumental Variables**

747 **mQTL allelic scores.** We identified 12,940 smoking-associated CpGs with *cis*-mQTL summary
748 statistics available from GoDMC¹⁸ (excluding NTR), using GoDMC’s definition of “*cis*” interval
749 (within 1Mb of the CpG). In GoDMC, the contributing cohorts performed genome-wide mQTL
750 analyses, testing the associations of ~480,000 CpG sites with ~12 million SNPs. However,

Causation between Smoking and DNA methylation

751 before the meta-analysis, the cohort-level results were filtered to retain the SNP-CpG pairs with
752 $p < 1 \times 10^{-5}$ within the cohort. Thus, since the summary statistics were already partly
753 thresholded, we computed the mQTL allelic scores by applying clumping and thresholding in
754 *PLINK1.9*⁵⁹. Linkage disequilibrium (LD)-based clumping was performed using `--clump-p1`
755 `1 --clump-kb 250`, with two levels of LD r^2 (0.5 and 0.1) specified for `--clump-r2`, thus
756 yielding two sets of LD-clumped *cis*-SNPs. Using either set of SNPs, we computed the allelic
757 score with `--score` at a threshold of 0.05 (applied with `--q-score-range`). If none of the
758 SNPs had $p < 0.05$, no threshold was applied for score calculation. An additional allelic score was
759 calculated using the top *cis*-mQTL (with the minimum association p-value) for each CpG. Thus,
760 for every CpG, three scores were calculated (two LD-clumped mQTL allelic scores, plus the top-
761 mQTL), though these scores were not necessarily distinct; for example, if a CpG had only one
762 *cis*-SNP, all three criteria yielded the same score. Likewise, for some CpGs, the two LD-
763 clumping cut-offs resulted in the same set of SNPs and, hence, identical mQTL allelic scores.

764

765 To assess the strength of an mQTL allelic score, we first estimated its incremental R^2 by fitting
766 generalized estimating equations (GEE), controlling for the standard EWAS covariates (as
767 above), genotyping platform, and the first ten genetic PCs. For each CpG, the effective GEE
768 sample size (N_{Eff}) was computed using the following formulae:

769

$$770 \quad N_{Eff}^{MZ} = \frac{2 * N_{MZ}}{1 + r_{MZ}}$$

771

$$772 \quad N_{Eff}^{DZ} = \frac{2 * N_{DZ}}{1 + r_{DZ}}$$

773

$$774 \quad N_{Eff} = N_{Eff}^{MZ} + N_{Eff}^{DZ} + N_{Ind}$$

775

776 where, N_{Eff}^{MZ} and N_{Eff}^{DZ} are the estimated effective sample sizes of MZ and DZ twins, N_{MZ} and
777 N_{DZ} are the numbers of complete MZ and DZ twin pairs, while r_{MZ} and r_{DZ} are the twin
778 phenotypic (DNAm) correlations in MZ and DZ twin pairs, respectively. N_{Ind} is the number of
779 individuals without the co-twin. The estimated effective sample size was then used to transform
780 the incremental R^2 value into an F-statistic as:

781

$$782 \quad F = \frac{R^2}{1 - R^2} \times \frac{N_{Eff} - K}{K - 1}$$

783

784 where $K = 2$, given two parameter estimates: the intercept and the regression coefficient of the
785 mQTL allelic score.

786

Causation between Smoking and DNA methylation

787 **PRS of Regular Smoking Initiation.** We used European-ancestry GWAS summary statistics for
788 smoking initiation (i.e., initiation of regular smoking) from the GWAS & Sequencing
789 Consortium of Alcohol and Nicotine use (GSCAN; excluding NTR)²⁰ to compute the PRS of
790 smoking in NTR using *LDpred v0.9*⁶⁰. Of note, the phenotypic definition in the GWAS (smoking
791 initiation = current/former versus never smoking) was different from the smoking phenotypes
792 (current versus never and former versus never smoking) in the MR-DoC models. However, in
793 these causal models, the strength of the IV, the extent of horizontal pleiotropy with DNAm, and
794 the estimated causal effects on DNAm are specific to the smoking phenotype used in the models.
795 As a result, this approach allowed us to assess the causal relationships of DNAm with current
796 and former smoking separately. See **Supplementary Methods** for a detailed description of PRS
797 calculation and estimation of incremental R². Using linear regression models, we residualized the
798 PRS of smoking and all mQTL allelic scores for the genotyping platform and the first ten genetic
799 PCs. The residuals were scaled to have a mean of zero and a variance of one before being
800 included as IVs in MR-DoC models.

801 MR-DoC Models

802 Causal inference in the twin *Direction-of-Causation* models uses the differences in cross-twin
803 cross-trait correlations under different directions of causation to identify the model that fits the
804 data best¹⁵. On the other hand, MR analyses rely on three assumptions of a valid IV^{3,19}, that the
805 IV is (1) associated with the exposure (“relevance”), (2) not correlated with any omitted
806 confounding variables (“exchangeability”), and (3) independent of the outcome, given the
807 exposure (“exclusion restriction”). Here, we used the criterion of F-statistic >10 to define the
808 “relevance” of the IV. Further, germline genetic variants are often assumed to satisfy the
809 “exchangeability” assumption due to Mendel’s laws of random segregation and independent
810 assortment. The “exclusion restriction” assumption for a genetic IV implies no horizontal
811 pleiotropy with the outcome. As described above, we relied on different specifications of MR-
812 DoC models to account for potential horizontal pleiotropy. MR-DoC1 model allowed estimating
813 and controlling for horizontal pleiotropy from the IV to the outcome, though it required us to fix
814 the unique environmental confounding at a specific value (here, zero)¹³. MR-DoC2 model
815 leverages the covariance between two polygenic or multiallelic IVs, beyond the bidirectional
816 causal effects, to partly accommodate horizontal pleiotropy¹⁴.

817
818 We used the *OpenMx* (version 2.21.8)⁶¹ package in R (version 4.3.2) to fit the MR-DoC models,
819 using the code provided in the original publications^{13,14}. Binary smoking status was examined
820 under the liability threshold model⁶², assuming a latent liability distribution with its mean fixed
821 at zero and variance fixed at one, while the threshold was freely estimated.

822
823 Before fitting the MR-DoC models, we examined univariate ACE twin models of smoking status
824 to estimate the additive genetic (A), shared environmental (C), and unique environmental (E)
825 variance components of the latent liability scale, with age and sex as covariates. Maximum-

Causation between Smoking and DNA methylation

826 likelihood tetrachoric correlation estimates for current versus never smoking were: $r_{MZ} = 0.925$
827 ($S.E. = 0.021$) in MZ pairs and $r_{DZ} = 0.533$ ($S.E. = 0.083$) in DZ pairs. Likewise, former
828 versus never smoking had $r_{MZ} = 0.822$ ($S.E. = 0.038$) and $r_{DZ} = 0.474$ ($S.E. = 0.096$). Based
829 on likelihood-ratio tests (LRT), an AE twin model was the most parsimonious model for both
830 current versus never (AE versus ACE LRT $p = 0.417$) and former versus never smoking (AE
831 versus ACE LRT $p = 0.530$) (**Supplementary Table S31**). The estimated variance components
832 of current versus never smoking liability were $A = 0.927$ (maximum-likelihood 95% confidence
833 interval: 0.879, 0.959) and $E = 0.073$ (0.041, 0.121). The corresponding estimates of former
834 versus never smoking were $A = 0.827$ (0.745, 0.888) and $E = 0.173$ (0.112, 0.255).

835
836 Prior twin analyses of DNAm at CpG sites in NTR⁵¹ showed that, of the 411,169 autosomal post-
837 QC CpG sites, the AE twin model was the best fitting model at all but 426 sites, with significant
838 (after multiple-testing correction of LRT p-values) C variance at 185 sites and significant non-
839 additive genetic (D) variance at 241 sites. Of the smoking-associated CpGs², only two CpGs had
840 significant estimates of C, while only seven CpGs had significant estimates of D. Thus, in MR-
841 DoC models, we specified an AE variance decomposition of DNAm at all smoking-associated
842 CpGs. Note that, in the results presented above, none of the CpG sites with consistent, nominally
843 significant estimates of causal effects in either direction (525 sites with *current smoking* \rightarrow
844 *DNAm*; 64 sites with *DNAm* \rightarrow *current smoking*) have significant C or D estimates per the
845 previous univariate twin analyses⁵¹. Moreover, since smoking status liability also has an AE
846 variance decomposition, including a C or D variance component of DNAm in the model would
847 not change the possible sources of covariance between smoking status and DNAm in the model.

848
849 We fitted five sets of MR-DoC models with current versus never smoking and similar sets with
850 former versus never smoking (**Figure 1**): (1) *Smoking* \rightarrow *DNAm* MR-DoC1 with horizontal
851 pleiotropy, (2) *Smoking* \rightarrow *DNAm* MR-DoC1 with unique environmental confounding, (3)
852 *DNAm* \rightarrow *Smoking* MR-DoC1 with horizontal pleiotropy, (4) *DNAm* \rightarrow *Smoking* MR-DoC1
853 with unique environmental confounding, and (5) bidirectional MR-DoC2. Each model included
854 age and sex as covariates of smoking status. In each model, the residual variance of smoking
855 status liability is decomposed into a_S^2 (A) and e_S^2 (E), while that of DNAm is decomposed into
856 a_D^2 (A) and e_D^2 (E). The correlation between the latent A factors of smoking and DNAm (r_A)
857 represents the confounding due to additive genetic factors. The correlation between the latent E
858 factors (r_E) represents the confounding due to unique environmental factors. Across all models,
859 the causal path from smoking to DNAm is labeled g_1 , while that from DNAm to smoking is
860 labeled g_2 . The residualized PRS and mQTL allelic scores are regressed on respective latent
861 factors, representing the underlying “true” standardized scores with mean fixed at zero and
862 variance fixed at one. The coefficient of the path from the latent score to the observed score
863 estimates the standard deviation of the observed score (SD_{PRS} and SD_{mQTL} , respectively).

864

Causation between Smoking and DNA methylation

865 Thus, for each CpG site included in the analyses, three causal estimates were obtained in either
866 direction (*Smoking* \rightarrow *DNAm*, or *DNAm* \rightarrow *Smoking*) from (1) MR-DoC1 with horizontal
867 pleiotropy, (2) MR-DoC1 with unique environmental confounding, and (3) MR-DoC2. For each
868 set of causal estimates across CpG sites, we calculated the Bayesian inflation factor (λ) using the
869 R package *bacon*²³, made QQ plots using the R package *GWASTools*⁶³, and then applied
870 Benjamini-Hochberg FDR correction⁶⁴ to the p-values using the R package *qvalue*⁶⁵. For
871 Bonferroni multiple-testing correction, the significance level was defined as $\alpha = 0.05/16940 =$
872 2.95×10^{-6} for *Current Smoking* \rightarrow *DNAm* MR-DoC1 models and $\alpha = 0.05/11124 =$
873 4.49×10^{-6} for *DNAm* \rightarrow *Current Smoking* MR-DoC1 and bidirectional current-smoking MR-
874 DoC2 models.

875 **Functional Enrichment Analyses**

876 We used Metascape²⁵ (v3.5.20240101; <https://metascape.org/gp/index.html#/main/step1>, with
877 the default settings for “Express” analyses) to perform gene-set annotation and functional
878 enrichment analyses of the CpGs with potential causal effects in either direction. The input list of
879 gene IDs was selected based on proximity to the CpGs with consistent and nominally significant
880 ($p < 0.05$) estimates in all three models; i.e., 64 CpGs with potential *DNAm* \rightarrow *Current Smoking*
881 effects (“Nearest Gene” in **Supplementary Table S3**) and 525 CpGs with potential *Current*
882 *Smoking* \rightarrow *DNAm* effects (“Nearest Gene” in **Supplementary Table S1**). None of the sites with
883 potential *DNAm* \rightarrow *Current Smoking* effects are located in the MHC region. For *Current*
884 *Smoking* \rightarrow *DNAm* effects, 21 additional sites in the MHC region showed consistent, nominally
885 significant estimates. There was no significant relationship between a CpG site having consistent
886 causal estimates and its being located in the MHC region (Fisher’s exact test p-value = 0.5455).
887 However, out of an abundance of caution, the sites located in this region were not included in the
888 enrichment analyses to avoid sites with potentially unreliable results due to its complex LD
889 structure.

890
891 As described in the Metascape manuscript²⁵, the program performed integrated enrichment
892 analyses against multiple reference ontology knowledgebases, including GO processes⁶⁶, KEGG
893 pathways⁶⁷, canonical pathways⁶⁸, and Reactome gene sets⁶⁹. The significant terms with a
894 hypergeometric p-value < 0.01 and > 1.5 -fold enrichment were clustered into a hierarchical tree
895 based on Kappa-statistical similarities among their gene memberships. The tree was then cast
896 into clusters based on a threshold of 0.3 kappa score to obtain enriched, non-redundant ontology
897 terms.

898 **eFORGE (experimentally derived Functional element Overlap analysis of** 899 **ReGions from EWAS)**

900 We performed *eFORGE 2.0*^{26,27,70} analyses of the selected CpG probe IDs with consistent and
901 nominally significant ($p < 0.05$) estimates in either direction (from **Supplementary Tables S1**,

Causation between Smoking and DNA methylation

902 **S3**). Using the web-based tool (<https://eforge.altiusinstitute.org/>), we examined the overlap
903 between the implicated CpGs and multiple comprehensive reference sets of genomic and
904 epigenomic features that regulate gene expression in different tissues and cell types. The
905 platform was set as “Illumina 450k array”, with default analysis options: proximity = 1kb
906 window, background repetitions = 1000, and significance thresholds of FDR <0.01 (strict) and
907 FDR <0.05 (marginal). Three sets of analyses were performed for each list of probe IDs,
908 selecting the reference data from “Consolidated Roadmap Epigenomics - Chromatin - All 15-
909 state marks”, “Consolidated Roadmap Epigenomics - DHS”, and “Consolidated Roadmap
910 Epigenomics - All H3 marks”.

911
912 The eFORGE results include the specific probe IDs overlapping between the input set and the
913 reference sample. We performed iterative follow-up analyses for the CpGs with potential *DNA_m*
914 → *Current Smoking* effects, based on the overlapping probe IDs to examine the specificity of
915 significant (FDR <0.01) enrichment in tissues of interest. Analyses restricted to the 21 CpGs
916 overlapping with enhancers in the fetal brain (**Supplementary Figure S18, Table S12**) showed
917 significant enrichment only for enhancers in the fetal brain samples, suggesting high specificity
918 (**Supplementary Figure S21**). The histone mark analyses also showed enrichment in the fetal
919 brain (though not specific to the brain), wherein all 21 CpGs overlapped with H3K4me1, while a
920 subset of 17 CpGs overlapped with H3K4me3 (**Supplementary Figure S22**). Finally, we
921 performed analyses restricted to these 17 CpGs.

922
923 We performed similar follow-up analyses with probe IDs showing overlap with enhancers in the
924 lung (potentially etiologically relevant tissue) and the primary B-cells in cord blood (the tissue
925 type with the most significant enrichment) (from **Supplementary Figure S18, Table S12**). We
926 also examined the overlap between the CpGs with potential *DNA_m* → *Current Smoking* effects
927 and the genes implicated in the GWAS of blood cell counts³⁷ to probe the potential impact of the
928 cell-count GWAS associations on the causal inference and cell-type enrichment. Similar overlap
929 was examined for the subset of CpGs overlapping with enhancers in cord blood primary B cells.
930

References

- 931
932
933 1. Wei, S. *et al.* Ten Years of EWAS. *Adv. Sci.* **8**, 2100727 (2021).
- 934 2. Joehanes, R. *et al.* Epigenetic Signatures of Cigarette Smoking. *Circ. Cardiovasc. Genet.* **9**,
935 436–447 (2016).
- 936 3. Lawlor, D. A., Harbord, R. M., Sterne, J. A., Timpson, N. & Davey Smith, G. Mendelian
937 randomization: using genes as instruments for making causal inferences in epidemiology.
938 *Stat Med* **27**, 1133–63 (2008).
- 939 4. Zillich, L. *et al.* Epigenetic Signatures of Smoking in Five Brain Regions. *J. Pers. Med.* **12**,
940 566 (2022).
- 941 5. Hannon, E. *et al.* An integrated genetic-epigenetic analysis of schizophrenia: evidence for
942 co-localization of genetic associations and differential DNA methylation. *Genome Biol.* **17**,
943 176 (2016).
- 944 6. Lohoff, F. W. *et al.* Epigenome-wide association study of alcohol consumption in N = 8161
945 individuals and relevance to alcohol use disorder pathophysiology: identification of the
946 cystine/glutamate transporter SLC7A11 as a top target. *Mol. Psychiatry* **27**, 1754–1764
947 (2022).
- 948 7. Fang, F. *et al.* Trans-ancestry epigenome-wide association meta-analysis of DNA
949 methylation with lifetime cannabis use. *Mol. Psychiatry* (2023) doi:10.1038/s41380-023-
950 02310-w.
- 951 8. Dhana, K. *et al.* An Epigenome-Wide Association Study of Obesity-Related Traits. *Am. J.*
952 *Epidemiol.* **187**, 1662–1669 (2018).

Causation between Smoking and DNA methylation

- 953 9. Davey Smith, G. & Ebrahim, S. Mendelian randomization: Can genetic epidemiology
954 contribute to understanding environmental determinants of disease? *Int J Epidemiol* **32**, 1–22
955 (2003).
- 956 10. Sun, Y.-Q. *et al.* Assessing the role of genome-wide DNA methylation between smoking and
957 risk of lung cancer using repeated measurements: the HUNT study. *Int. J. Epidemiol.* **50**,
958 1482–1497 (2021).
- 959 11. Jamieson, E. *et al.* Smoking, DNA Methylation, and Lung Function: A Mendelian
960 Randomization Analysis to Investigate Causal Pathways. *Am. J. Hum. Genet.* **106**, 315–326
961 (2020).
- 962 12. Burgess, S., Thompson, S. G. & CRP CHD Genetics Collaboration. Avoiding bias from
963 weak instruments in Mendelian randomization studies. *Int J Epidemiol* **40**, 755–64 (2011).
- 964 13. Minică, C. C., Dolan, C. V., Boomsma, D. I., De Geus, E. & Neale, M. C. Extending
965 Causality Tests with Genetic Instruments: An Integration of Mendelian Randomization with
966 the Classical Twin Design. *Behav. Genet.* **48**, 337–349 (2018).
- 967 14. Castro-de-Araujo, L. F. S. *et al.* MR-DoC2: Bidirectional Causal Modeling with
968 Instrumental Variables and Data from Relatives. *Behav. Genet.* **53**, 63–73 (2023).
- 969 15. Heath, A. C. *et al.* Testing hypotheses about direction of causation using cross-sectional
970 family data. *Behav. Genet.* **23**, 29–50 (1993).
- 971 16. Minică, C. C., Boomsma, D. I., Dolan, C. V., De Geus, E. & Neale, M. C. Empirical
972 comparisons of multiple Mendelian randomization approaches in the presence of assortative
973 mating. *Int. J. Epidemiol.* **49**, 1185–1193 (2020).
- 974 17. Ligthart, L. *et al.* The Netherlands Twin Register: Longitudinal Research Based on Twin and
975 Twin-Family Designs. *Twin Res. Hum. Genet.* **22**, 623–636 (2019).

Causation between Smoking and DNA methylation

- 976 18. Min, J. L. *et al.* Genomic and phenotypic insights from an atlas of genetic effects on DNA
977 methylation. *Nat. Genet.* **53**, 1311–1321 (2021).
- 978 19. Richmond, R. C. & Davey Smith, G. Mendelian Randomization: Concepts and Scope. *Cold*
979 *Spring Harb Perspect Med* (2021) doi:10.1101/cshperspect.a040501.
- 980 20. Saunders, G. R. B. *et al.* Genetic diversity fuels gene discovery for tobacco and alcohol use.
981 *Nature* **612**, 720–724 (2022).
- 982 21. Bibikova, M. *et al.* High density DNA methylation array with single CpG site resolution.
983 *New Genomic Technol. Appl.* **98**, 288–295 (2011).
- 984 22. Falconer, D. S. *Introduction To Quantitative Genetics*. (Oliver and Boyd, Edinburgh, 1960).
- 985 23. van Iterson, M., van Zwet, E. W., Heijmans, B. T., & the BIOS Consortium. Controlling bias
986 and inflation in epigenome- and transcriptome-wide association studies using the empirical
987 null distribution. *Genome Biol.* **18**, 19 (2017).
- 988 24. Castro-de-Araujo, L. F. *et al.* Power, measurement error, and pleiotropy robustness in twin-
989 design extensions to Mendelian Randomization. *Research square* rs.3.rs-3411642 Preprint at
990 <https://doi.org/10.21203/rs.3.rs-3411642/v1> (2023).
- 991 25. Zhou, Y. *et al.* Metascape provides a biologist-oriented resource for the analysis of systems-
992 level datasets. *Nat. Commun.* **10**, (2019).
- 993 26. Breeze, C. E. *et al.* eFORGE: A Tool for Identifying Cell Type-Specific Signal in
994 Epigenomic Data. *Cell Rep.* **17**, 2137–2150 (2016).
- 995 27. Breeze, C. E. *et al.* eFORGE v2.0: updated analysis of cell type-specific signal in
996 epigenomic data. *Bioinformatics* **35**, 4767–4769 (2019).
- 997 28. Edenberg, H. J. *et al.* Genome-Wide Association Study of Alcohol Dependence Implicates a
998 Region on Chromosome 11. *Alcohol. Clin. Exp. Res.* **34**, 840–852 (2010).

Causation between Smoking and DNA methylation

- 999 29. Khan, A. H. *et al.* Genetic pathways regulating the longitudinal acquisition of cocaine self-
1000 administration in a panel of inbred and recombinant inbred mice. *Cell Rep.* **42**, 112856
1001 (2023).
- 1002 30. Jin, X., Dong, S., Yang, Y., Bao, G. & Ma, H. Nominating novel proteins for anxiety via
1003 integrating human brain proteomes and genome-wide association study. *J. Affect. Disord.*
1004 **358**, 129–137 (2024).
- 1005 31. Sarkar, A. *et al.* Hippocampal HDAC4 Contributes to Postnatal Fluoxetine-Evoked
1006 Depression-Like Behavior. *Neuropsychopharmacology* **39**, 2221–2232 (2014).
- 1007 32. Aldosary, M. *et al.* SLC25A42-associated mitochondrial encephalomyopathy: Report of
1008 additional founder cases and functional characterization of a novel deletion. *JIMD Rep.* **60**,
1009 75–87 (2021).
- 1010 33. Stankiewicz, A. M., Jaszczyk, A., Goscik, J. & Juszczak, G. R. Stress and the brain
1011 transcriptome: Identifying commonalities and clusters in standardized data from published
1012 experiments. *Prog. Neuropsychopharmacol. Biol. Psychiatry* **119**, 110558 (2022).
- 1013 34. Cochran, J. N. *et al.* Genetic associations with age at dementia onset in the PSEN1 E280A
1014 Colombian kindred. *Alzheimers Dement.* **19**, 3835–3847 (2023).
- 1015 35. Mahajan, U. V. *et al.* Dysregulation of multiple metabolic networks related to brain
1016 transmethylation and polyamine pathways in Alzheimer disease: A targeted metabolomic
1017 and transcriptomic study. *PLOS Med.* **17**, e1003012 (2020).
- 1018 36. Blanco-Luquin, I. *et al.* Early epigenetic changes of Alzheimer’s disease in the human
1019 hippocampus. *Epigenetics* **15**, 1083–1092 (2020).
- 1020 37. Vuckovic, D. *et al.* The Polygenic and Monogenic Basis of Blood Traits and Diseases. *Cell*
1021 **182**, 1214–1231.e11 (2020).

Causation between Smoking and DNA methylation

- 1022 38. Dugué, P.-A. *et al.* Smoking and blood DNA methylation: an epigenome-wide association
1023 study and assessment of reversibility. *Epigenetics* **15**, 358–368 (2020).
- 1024 39. van Dongen, J. *et al.* Effects of smoking on genome-wide DNA methylation profiles: A
1025 study of discordant and concordant monozygotic twin pairs. *eLife* **12**, e83286 (2023).
- 1026 40. Pidsley, R. *et al.* Critical evaluation of the Illumina MethylationEPIC BeadChip microarray
1027 for whole-genome DNA methylation profiling. *Genome Biol.* **17**, 208 (2016).
- 1028 41. Wong, T.-S. *et al.* G protein-coupled receptors in neurodegenerative diseases and psychiatric
1029 disorders. *Signal Transduct. Target. Ther.* **8**, 177 (2023).
- 1030 42. Stankiewicz, A. M. *et al.* Novel candidate genes for alcoholism — transcriptomic analysis of
1031 prefrontal medial cortex, hippocampus and nucleus accumbens of Warsaw alcohol-preferring
1032 and non-preferring rats. *Pharmacol. Biochem. Behav.* **139**, 27–38 (2015).
- 1033 43. Burchett, S. A., Bannon, M. J. & Granneman, J. G. RGS mRNA Expression in Rat Striatum.
1034 *J. Neurochem.* **72**, 1529–1533 (1999).
- 1035 44. Chen, X. *et al.* Structural basis for recruitment of TASL by SLC15A4 in human
1036 endolysosomal TLR signaling. *Nat. Commun.* **14**, 6627 (2023).
- 1037 45. Kobayashi, T. *et al.* Lysosome biogenesis regulated by the amino-acid transporter SLC15A4
1038 is critical for functional integrity of mast cells. *Int. Immunol.* **29**, 551–566 (2017).
- 1039 46. Teschendorff, A. E. *et al.* Correlation of Smoking-Associated DNA Methylation Changes in
1040 Buccal Cells With DNA Methylation Changes in Epithelial Cancer. *JAMA Oncol.* **1**, 476–
1041 485 (2015).
- 1042 47. Simpson, J. T. *et al.* Detecting DNA cytosine methylation using nanopore sequencing. *Nat.*
1043 *Methods* **14**, 407–410 (2017).

Causation between Smoking and DNA methylation

- 1044 48. Evans, D. M., Gillespie, N. A. & Martin, N. G. Biometrical genetics. *Biol. Psychol.* **61**, 33–
1045 51 (2002).
- 1046 49. Illumina, Inc. Infinium Methylation Screening Array-48 Kit. (2024).
- 1047 50. Willemsen, G. *et al.* The Netherlands Twin Register Biobank: A Resource for Genetic
1048 Epidemiological Studies. *Twin Res. Hum. Genet.* **13**, 231–245 (2010).
- 1049 51. van Dongen, J. *et al.* Genetic and environmental influences interact with age and sex in
1050 shaping the human methylome. *Nat. Commun.* **7**, 11115 (2016).
- 1051 52. Singh, M. *et al.* Using Instrumental Variables to Measure Causation over Time in Cross-
1052 Lagged Panel Models. *Multivar. Behav. Res.* **59**, 342–370 (2024).
- 1053 53. van Iterson, M. *et al.* MethylAid: visual and interactive quality control of large Illumina 450k
1054 datasets. *Bioinformatics* **30**, 3435–3437 (2014).
- 1055 54. Sinke, L., van Iterson, M., Cats, D., Slieker, R. & Heijmans, B. DNAmArray: Streamlined
1056 workflow for the quality control, normalization, and analysis of Illumina methylation array
1057 data. Zenodo <https://doi.org/10.5281/zenodo.3355292> (2019).
- 1058 55. Fortin, J.-P. *et al.* Functional normalization of 450k methylation array data improves
1059 replication in large cancer studies. *Genome Biol.* **15**, 503 (2014).
- 1060 56. Francioli, L. C. *et al.* Whole-genome sequence variation, population structure and
1061 demographic history of the Dutch population. *Nat. Genet.* **46**, 818–825 (2014).
- 1062 57. van Rooij, J. *et al.* Evaluation of commonly used analysis strategies for epigenome- and
1063 transcriptome-wide association studies through replication of large-scale population studies.
1064 *Genome Biol.* **20**, 235 (2019).
- 1065 58. van Dongen, J. *et al.* DNA methylation signatures of educational attainment. *Npj Sci. Learn.*
1066 **3**, 7 (2018).

Causation between Smoking and DNA methylation

- 1067 59. Chang, C. C. *et al.* Second-generation PLINK: rising to the challenge of larger and richer
1068 datasets. *GigaScience* **4**, s13742-015-0047–8 (2015).
- 1069 60. Vilhjálmsson, J. *et al.* Modeling Linkage Disequilibrium Increases Accuracy of Polygenic
1070 Risk Scores. *Am. J. Hum. Genet.* **97**, 576–592 (2015).
- 1071 61. Neale, M. C. *et al.* OpenMx 2.0: Extended Structural Equation and Statistical Modeling.
1072 *Psychometrika* **81**, 535–549 (2016).
- 1073 62. Verhulst, B. & Neale, M. C. Best Practices for Binary and Ordinal Data Analyses. *Behav.*
1074 *Genet.* **51**, 204–214 (2021).
- 1075 63. Gogarten, S. M. *et al.* GWASTools: an R/Bioconductor package for quality control and
1076 analysis of genome-wide association studies. *Bioinformatics* **28**, 3329–3331 (2012).
- 1077 64. Benjamini, Y. & Hochberg, Y. Controlling the False Discovery Rate: A Practical and
1078 Powerful Approach to Multiple Testing. *J. R. Stat. Soc. Ser. B Methodol.* **57**, 289–300
1079 (1995).
- 1080 65. Storey, J., Bass, A., Dabney, A. & Robinson, D. qvalue: Q-value estimation for false
1081 discovery rate control. doi:10.18129/B9.bioc.qvalue. (2023).
- 1082 66. Ashburner, M. *et al.* Gene Ontology: tool for the unification of biology. *Nat. Genet.* **25**, 25–
1083 29 (2000).
- 1084 67. Kanehisa, M. & Goto, S. KEGG: Kyoto Encyclopedia of Genes and Genomes. *Nucleic Acids*
1085 *Res.* **28**, 27–30 (2000).
- 1086 68. Subramanian, A. *et al.* Gene set enrichment analysis: A knowledge-based approach for
1087 interpreting genome-wide expression profiles. *Proc. Natl. Acad. Sci.* **102**, 15545–15550
1088 (2005).

Causation between Smoking and DNA methylation

- 1089 69. Fabregat, A. *et al.* The Reactome Pathway Knowledgebase. *Nucleic Acids Res.* **46**, D649–
1090 D655 (2018).
- 1091 70. Breeze, C. E. Cell Type-Specific Signal Analysis in Epigenome-Wide Association Studies.
1092 in *Epigenome-Wide Association Studies: Methods and Protocols* (ed. Guan, W.) 57–71
1093 (Springer US, New York, NY, 2022). doi:10.1007/978-1-0716-1994-0_5.
1094